Bohrson WA, Spera FJ, Heinonen JS, Brown GA, Scruggs MA, Adams JV, Takach M, Zeff G, Suikkanen E (2020) Diagnosing Open-System Magmatic Processes Using the Magma Chamber Simulator (MCS): Part I - Major Elements and Phase Equilibria. Contributions to Mineralogy and Petrology 175:104. https://doi.org/10.1007/s00410-020-01722-z (Author's postprint)

Diagnosing Open-System Magmatic Processes Using the Magma Chamber Simulator (MCS): Part I - Major Elements and Phase Equilibria

Wendy A. Bohrson[1,2], Frank J. Spera[3], Jussi S. Heinonen[1,4], Guy A. Brown[5], Melissa A. Scruggs[3], Jenna V. Adams[3], Marie Takach[1]*, Garrett Zeff[3]**, Einari Suikkanen[4]

[1]Department of Geological Sciences, Central Washington University, Ellensburg, WA. 98926 USA,
[2]Department of Geology and Geological Engineering, Colorado School of Mines, Golden, CO, 80401 USA https://orcid.org/0000-0002-2611-6402
[3]Department of Earth Science and Earth Research Institute, University of California, Santa Barbara, CA. 93106 USA
[4]Department of Geosciences and Geography, University of Helsinki, P.O. Box 64, 00014 Helsinki, Finland
[5]Rocking Hoarse Professional Services, 691 Chelham Way, Santa Barbara, CA. 93108 USA
*Present address: College of Earth, Ocean, and Atmospheric Sciences, Oregon State University, Corvallis, OR 97311
**Present address: Earth & Planetary Sciences, University of California, Santa Cruz, CA. 95064

Abstract

The Magma Chamber Simulator (MCS) is a thermodynamic tool for modeling the evolution of magmatic systems that are open with respect to assimilation of partial melts or stoped blocks, magma recharge + mixing, and fractional crystallization. MCS is available for both PC and Mac. In the MCS, the thermal, mass, and compositional evolution of a multicomponent–multiphase composite system of resident magma, wallrock, and recharge reservoirs is tracked by rigorous self-consistent thermodynamic modeling. A Recharge–Assimilation (Assimilated partial melt or Stoped blocks)–Fractional Crystallization (R_nAS_nFC; $n_{tot} \leq 30$) scenario is computed by minimization or maximization of appropriate thermodynamic potentials using the family of rhyolite- and pMELTS engines coupled to an Excel Visual Basic interface. In MCS, during isobaric cooling and crystallization, resident magma thermally interacts with wallrock that is in internal thermodynamic equilibrium. Wallrock partial melt above a user-defined percolation threshold is homogenized (i.e., brought in to chemical potential equilibrium) with resident magma. Crystals that form become part of a cumulate reservoir that remains thermally connected but chemically isolated from resident melt. Up to 30 instances ($n \leq 30$) of magma mixing by recharge and/or bulk assimilation of stoped wallrock blocks can occur in a single simulation; each recharge magma or stoped block has a unique user-defined composition and thermal state. Recharge magmas and stoped blocks hybridize (equilibrate) with resident melt, yielding a single new melt composition and temperature. MCS output includes major and trace element concentrations and isotopic ratios (Sr, Nd, Hf, Pb, Os, and O as defaults) of wallrock, recharge magma/stoped blocks, resident magma melt, and cumulates. The chemical formulae of equilibrium crystalline phases in the cumulate reservoir, wallrock, and recharge magmas/stoped blocks are also output. Depending on the selected rhyolite-MELTS engine, the composition and properties of a

possible supercritical fluid phase (H_2O and/or CO_2) are also tracked. Forward modeling of theoretical magma systems and suites of igneous rocks provides quantitative insight into key questions in igneous petrology such as mantle versus crustal contributions to terrestrial magmas, the record of magmatism preserved in cumulates and exsolved fluids, and the chronology of RASFC processes that may be recorded by crystal populations, melt inclusions, and whole rocks. Here, we describe the design of the MCS software that focuses on major element compositions and phase equilibria (MCS-PhaseEQ). Case studies that involve fractional crystallization, magma recharge + mixing, and crustal contamination of a depleted basalt that resides in average upper crust illustrate the major element and phase equilibria consequences of these processes and highlight the rich array of data produced by MCS. The cases presented here, which represent an infinitesimal fraction of possible RASFC processes and bulk compositions, show that the records of recharge and/or crustal contamination may be subtle and are not necessarily those that would be predicted using conventional intuition and simple mass balance arguments. Mass and energy constrained thermodynamic tools like the MCS quantify the open-system evolution of magmas and provide a systematic understanding of the petrology and geochemistry of open system magmatic processes. The trace element and isotope MCS computational tool (MCS-Traces) is described in a separate contribution (part II).

Key words: Magma Chamber Simulator, open-system magma processes, modeling, magma differentiation, thermodynamics

Introduction

Studies of igneous rocks provide evidence that magmas evolve as open systems where exchange of matter and energy occurs at a range of spatial and temporal scales. Since the 1950s, improvements in geochemical instrumentation have enabled high precision analyses of igneous products (e.g., melts and fluid inclusions, single crystals, populations of crystals) at increasingly smaller spatial and temporal scales. These analytical advancements have led to many new insights into the complexities of how magmas evolve and aggregate. To fully utilize the enormous potential afforded by such data sets, a parallel advancement in computational modeling is a logical complement.

Trace element and isotopic models of open system magma processes have evolved from earlier studies that focused on mass balance (e.g., Taylor 1980; DePaolo 1981 and others) to those that incorporated mass and energy balance in the context of open system evolution (e.g., Spera and Bohrson 2001; Bohrson and Spera 2001, and references therein). Thermodynamic modeling has also progressed in important ways, and present-day models such as the family of rhyolite-MELTS models (Ghiorso and Sack 1995; Asimow and Ghiorso 1998; Gualda et al. 2012; Ghiorso and Gualda 2015), pMELTS (Ghiorso et al. 2002) and THERMOCALC (e.g., Powell and Holland 1988, 1994; Powell et

al. 1998) provide tools for documenting mineral-melt-fluid phase equilibria in differentiating magmatic systems. In this contribution, we present the Magma Chamber Simulator (MCS; Bohrson et al. 2014) as a versatile computational tool for the igneous petrologist/geochemist. MCS utilizes the MELTS family of models to combine thermodynamic constraints on melt-solid–fluid equilibria with mass and energy conservation for a composite open magma undergoing magma mixing via recharge, crustal assimilation via wallrock partial melting and stoping, and fractional crystallization. Model output includes compositional, isotopic, mass, and thermal data on all melts, solids, and fluid in each subsystem.

MCS is a forward modeling tool (discussion of both forward and inverse modeling in geochemistry may be found in Albarede 1995) that can serve in several ways to elucidate the evolution of magmatic systems. Forward modeling helps to understand how variations in the values of specific parameters (e.g., pressure, parental magma composition, wallrock initial temperature, number and mass of recharge events) affect the course of magmatic system evolution. This approach enables one to obtain an intuitive understanding of open system magmatic processes, including a basis for concluding which variables have the largest effect. Forward modeling is also useful when attempting to model a particular natural system. In this case, one can adjust input parameters to best reproduce petrological and geochemical data from a particular suite of igneous rocks. Understanding the sensitivity of the solution to input parameters is especially important when modeling natural systems, because the investigator is often confronted with significant uncertainties.

The use of MCS to both build intuition and to model data from individual volcanic or plutonic systems addresses a range of goals in the study of igneous rocks. Among the questions that can be addressed by MCS are how does the balance of mantle and crust change with time in a particular magmatic system; are there systematic differences in mantle versus crustal input in different tectonic settings (e.g., Cox and Hawkesworth 1984; Asmerom et al. 1991; Moore et al. 2018); what influences where magma storage zones form (shallow versus middle versus deep crust, e.g., Walker et al. 1993; Mangiacapra et al. 2008; Becerril et al. 2013; Weber and Castro 2017); what conditions favor large versus small magma bodies; and what processes and/or conditions modeled by MCS influence magma bodies to erupt (e.g., Tepley et al. 2000, 2013; Wark et al. 2007; Scruggs and Putirka 2018; Ubide and Kamber 2018)?

In this contribution, we provide an overview of the design of the major element and phase equilibria part of the code (MCS-PhaseEQ); the trace element and isotope part of MCS (MCS-Traces) will be discussed in a companion paper (Heinonen et al. 2020). We also highlight the utility of forward modeling by providing a comparison of cases that illustrate the petrologic and geochemical consequences of five recharge, assimilation, stoping, fractional crystallization (RASFC) scenarios (FC, R_2FC, AFC, S_2FC, and R_2AFC where the subscript defines the number of "events"). The results of these models provide perspective on how melt + crystals + fluid in a crustal magma system may

evolve in response to different combinations of open-system processes. Presentation of these models also serves to illustrate the rich array of results that MCS produces and how these results may be used to distinguish different open system scenarios (e.g., presence or absence or magma recharge, stoping versus assimilation of anatectic melt). In the companion paper, trace element and isotopic characteristics for these same five cases are presented along with the theory and code logistics for MCS-Traces. Examples of the use of MCS in studies of natural systems are given elsewhere (e.g., Borisova et al. 2017; Takach 2018, Heinonen et al. 2019).

Design of the Magma Chamber Simulator

What is the Magma Chamber Simulator?

The Magma Chamber Simulator is a thermodynamic model that quantifies the evolution of an open composite magmatic system composed of four subsystems: resident magma, cumulate reservoir, wallrock, and distinct recharge reservoirs. These subsystems interact by exchange of matter and energy following the constraints imposed by local thermodynamic equilibrium, as described below. MCS models simultaneous fractional crystallization, contamination by partial melt assimilation (AFC in the MCS jargon) and stoping (S, SFC in the MCS jargon), and magma mixing by recharge (RFC in the MCS jargon).

In MCS, the resident Magma subsystem (M), initially, a finite mass of melt in a well-defined thermodynamic state, is coupled to its host Wallrock (WR) via a diabatic and semi-permeable boundary. During AFC processes, sensible (melt cooling) and latent heat (formation of cumulates by fractional crystallization, FC) flows across the M–WR boundary, heating up and potentially partially melting wallrock. If partial melt forms and the melt fraction in wallrock exceeds a rheologically determined, user-specified critical threshold (f_m^o or FmZero), this anatectic melt thoroughly mixes and equilibrates with melt in the M subsystem (called M melt for brevity). Crystals that form in response to AFC become part of a cumulate reservoir that is thermally connected to but chemically isolated from M melt. The extent of matter transfer between WR and M is governed by key parameters connected to ambient geological conditions and initial bulk compositions (Tables 1, 2, e.g., is WR cold or warm, wet or dry, gabbroic or granitic)? In addition to contamination of M melt by wallrock partial melt, contamination can occur by the process of stoping (S). In MCS, stoped wallrock is added *en masse* to M melt, and the contaminated system comes to a new equilibrium state at a new thermodynamically controlled temperature. The stoping event may cause crystalline solids or a fluid to precipitate, and naturally, the contaminated M melt assumes a different bulk composition. A final process that MCS accounts for is magma mixing by recharge (R). During R, a finite mass of internally equilibrated recharge magma, in a well-defined thermodynamic state, is added to M melt, and the new

mixture attains chemical potential equilibrium. This operation is computationally identical to the stoping operation. The user-defined condition that triggers an R or S event is either a specified M melt temperature or a temperature decrement from the last S or R event. The current version of MCS allows a total of up to 30 distinct events of the S or R type. For more information about the theoretical underpinnings of MCS, the reader is directed to Bohrson et al. (2014).

Table 1. System variables and compositions of parent magma, recharge magmas, wallrock and stoped blocks for five MCS simulations

System Variables	
Pressure (GPa)	0.1
Percolation Threshold	0.1
*f*O2 (during simulation)	none/absent

Compositions		
Oxide in Wt. %	Parental (Resident) and Recharge Magma Composition	Wallrock and Stoped Block Composition
SiO2	49.38	64.53
TiO2	1.73	0.62
Al2O3	13.79	14.92
Fe2O3 [a,b]	1.83	1.3
Cr2O3	0	0
FeO [a, b]	8.73	3.71
MnO	0.18	0.1
MgO	7.82	2.4
NiO	0	0
CoO	0	0
CaO	12.09	3.48
Na2O	2.12	3.17
K2O	0.23	2.71
P2O5	0.15	0.15
H2O	1.96*	1.94
CO2	0.00	0.97

[a]For the parent magma, Fe^{2+}/Fe^{3+} was calculated at FMQ at 1129 °C and at 0.1 GPa after adding ~ 2 wt.% of H_2O. Following this fO_2 calculation, the magma composition was normalized to 100%. See text for additional discussion.

[b]For the WR, Fe^{2+}/Fe^{3+} was calculated at FMQ at 740° C and at 0.1 GPa after adding ~ 2 wt.% of H_2O and ~ 1 wt.% of CO_2; following this fO_2 calculation, the WR composition was normalized to 100%. See text for additional discussion.

Table 2. Initial conditions for five MCS simulations

	FC	**R2FC**	**AFC**	**S2FC**	**R2AFC**
Magma Liquidus Temperature (°C)[a]	1129	1129	1129	1129	1129
Temperature Decrement (°C)	5	5	5	5	5
Magma Initial Mass (expressed as mass units, m.u.)	100	100	100	100	100
Hard Stop Temperature (°C)[b]	900	900	800	900	800
Wallrock Find Solidus Start Temperature (°C)[c]	880	880	880	880	880
Wallrock Find Solidus End Temperature (°C)[c]	700	700	700	700	700
Wallrock Find Solidus Temperature Decrement (°C)[c]	5	5	5	5	5
Wallrock Initial temperature (°C)	100	100	700	100	700
Wallrock Initial Mass (m.u.)	200	200	200	200	200
Recharge/Stope Event 1: Mass (m.u.)		75		17	75
Recharge/Stope Event 1: Temperature of Recharge/Stoped Block When Recharge/Stoping Occurs (°C)[d]		1130		760	1130
Recharge/Stope Event 1: Temperature of Magma When Recharge/Stoping Occurs (°C)[e]		1050		1015	1050
Recharge/Stope Event 2: Mass (m.u.)		75		38	75
Recharge/Stope Event 2: Temperature of Recharge/Stoped Block When Recharge/Stoping Occurs (°C)[d]		1080		795	1080
Recharge/Stope Event 2: Temperature of Magma When Recharge/Stoping Occurs (°C) [e]		1000		908	1000

[a]Hard stop temperature is temperature at which simulation ends, if this temperature is achieved prior to wallrock and magma reaching thermal equilibrium

[b]These parameters represent the starting and ending temperatures and the temperature decrement that are used in the wallrock find solidus routine of MCS. See https://mcs.geol.ucsb.edu for more information

[c]This represents the temperature of the recharge magma/stoped block when it enters the M melt

[d]This represents the temperature of the resident magma (M melt and cumulates) when the recharge/stoping event occurs. Note that the temperature at which recharge actually occurs (e.g., ~ 1049 °C for R1 in R_2FC case) differs slightly from that reported in the input (1050 °C), because the recharge event occurs in the step after that target temperature is reached

How does the Magma Chamber Simulator Computer Code Work?

The MCS calculations are undertaken in two parts: (1) MCS-PhaseEQ: the major element and phase equilibria computation of the RASFC evolution, and (2) MCS-Traces: the trace element and isotopic (Sr, Nd, Hf, Pb, Os, and O) consequences of the RASFC scenario from output of MCS-PhaseEQ. This bipartite structure recognizes that robust trace element/isotopic calculations are necessarily built upon an accurate major element solution that quantifies phase abundances, compositions, and temperatures. A researcher may iterate in step (1) by comparing observables with predicted results before investing effort into trace element and isotopic modeling. Conversely, because of the bipartite structure, a researcher can run multiple trace element and isotopic ratio calculations using, for example, different initial trace element compositions and/or mineral–melt, mineral–fluid partition coefficients for M, WR, S and R utilizing the same part (1) RASFC solution. Feedback to MCS-PhaseEQ for different trace element concentrations and isotopic ratios is not required, because major phase stability is not typically sensitive to trace elements. The bipartite approach maintains maximal flexibility in the pursuit of a 'best-fit' model and aids in understanding the sensitivity of a full solution (phase equilibria, trace elements and isotope) to the initial conditions and parameters.

MCS-PhaseEQ is the union between a computational thermodynamic engine and an executive brain (Bohrson et al., 2014). The executive brain is built with Microsoft's Visual Basic programming language; a snapshot of the user interface of the current version is presented in Fig. 1. The brain is responsible for implementing the particular R_nAS_nFC scenario specified by the user by (1) sending instructions to the chosen rhyolite- or pMELTS engine, (2) performing additional internal calculations based on values returned from rhyolite- or pMELTS, (3) making the conditional and complex sequential executive decisions required to carry out the user-defined R_nAS_nFC petrological scenario, (4) producing a variety of real-time and archived graphical and numerical output, and (5) archiving input and output in a systematic manner enabling a synoptic view of the results. Several separate tools are available from the MCS website to mine and utilize the output for various purposes.

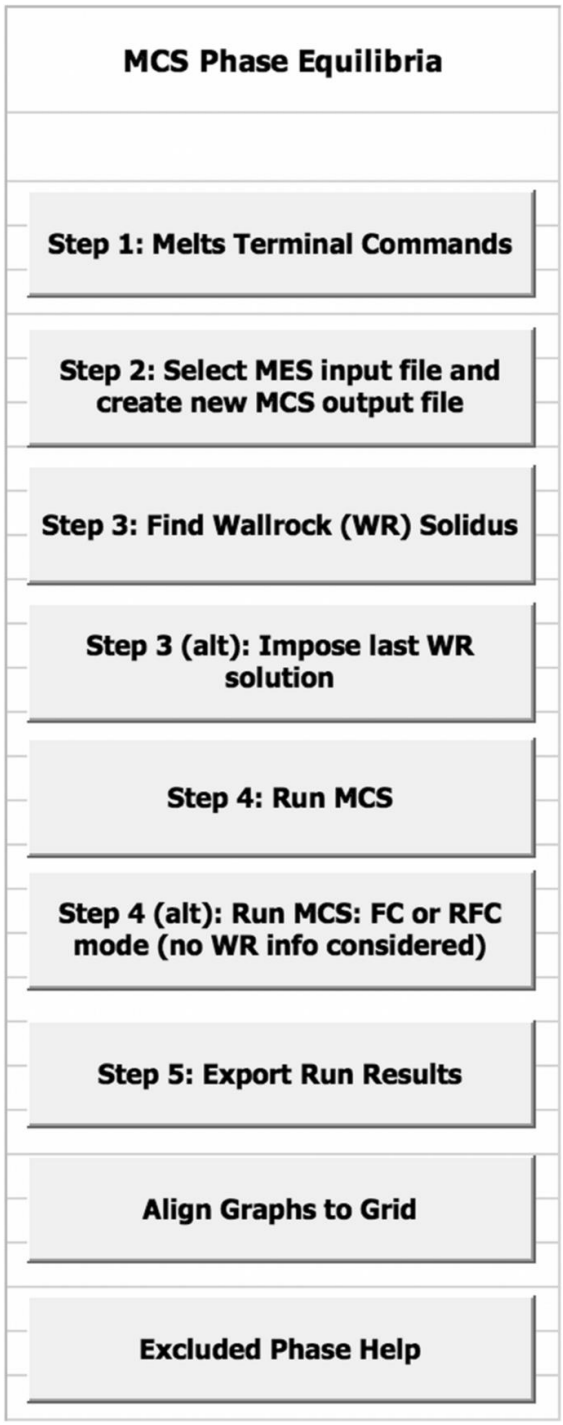

Figure 1. Command functions in the phase equilibria/major element interface of MCS-PhaseEQ. Step 1 initiates MCS communication with rhyolite- or pMELTS. Step 2 involves choosing an output file name and input MES file from those available. Step 3 is a preliminary calculation that prepares the WR subsystem by computing a solidus or near solidus thermodynamic state for wallrock for eventual coupling with the M subsystem, a requirement for AFC scenarios. Step 4 launches and runs the MCS-PhaseEQ simulation. Step 5 involves exporting the simulation results to an Excel workbook (see Online Resource 6). The other steps provide enhanced capability for running MCS, and these are detailed on the MCS website.

The thermodynamic engine implemented in the MCS-PhaseEQ is one of the rhyolite- or pMELTS codes currently available. These are enumerated as pMELTS, and rhyolite-MELTS versions 1.0.2, 1.1.0, or 1.2.0 (Ghiorso and Sack 1995; Asimow and Ghiorso 1998; Ghiorso et al. 2002; Gualda et al. 2012; Ghiorso and Gualda 2015; https://melts.ofm-research.org/). A centerpiece of rhyolite- or pMELTS is a thermodynamic model for the dependence of Gibbs free energy of silicate liquids as a function of melt composition, temperature (roughly 1000–2000 K), and pressure (roughly 0–3 GPa). For numerical calculations, the laws of thermodynamics, which are adhered to in rhyolite- and pMELTS are not sufficient, and must be adjoined with the thermodynamic properties of the materials composing the composite system.

More about Critical Design Features of Magma Chamber Simulator

MCS was designed as a thermodynamic model that has built-in assumptions about the ways in which the subsystems interact. Like all models, the design of MCS leads to limitations in its application to natural systems and to developing a framework for understanding how RASFC processes, in all their complexity. In this section, we enumerate key aspects of the design features of MCS and highlight limitations in its use.

First and perhaps foremost, as noted, MCS is a thermodynamic model that, while allowing for open system behavior, assumes local thermodynamic equilibrium. There are no compositional, pressure, temperature or other gradients within wallrock, magma or recharge reservoirs. Because MCS is a thermodynamic and not a transport model, thorough and complete homogenization is assumed when magmas mix, blocks are stoped, or partial melts are assimilated. Heat and matter are instantaneously exchanged between wallrock, magma (melt + cumulates) and recharge/stoping subsystems, and each subsystem is, therefore, characterized by a uniform temperature in each "step" of a simulation. Enthalpy is conserved, and thus the temperature of the M melt and cumulate subsystems is affected not only by temperature decrements imposed by user-defined cooling (see below), but also by adjustments required by addition of hotter or colder recharge magma or wallrock stoped blocks or anatectic melt.

In MCS, no absolute timescale is defined. However, an MCS 'arrow of time' (i.e., sequence of events) is defined by a user-specified RASFC scenario. Output archives an evolutionary record of melt composition, cumulate petrology, anatectic melt composition, wallrock residual mineralogy, and pre-mixing state of stoped blocks and recharge magmas. Quantification of timescales can be approximated using simple scaling arguments based on observed features such as mineral zoning and magma mixing times (e.g., Oldenburg et al. 1989; Costa et al. 2008; Spera et al. 2016) in consort with MCS results. A critic might object to the purely thermodynamic approach noting that many irreversible processes with concomitant entropy production (heat conduction and convection,

chemical diffusion, transport of momentum by the action of viscosity) surely come into play during the evolution of magmatic systems. We would not argue against this vantage. However, experience shows that local equilibrium is indeed often attained in high-temperature petrologic systems. Both the existence of a host of useful geothermometers, geobarometers, and geohygrometers (e.g., Putirka 2008, 2017; Wade et al. 2008; Coogan et al. 2014; Neave and Putirka 2017) and the consistency of laboratory experiments with observed features in natural magmatic systems (e.g., Bowen 1928; Yoder and Tilley 1962; Grove et al. 1992; Villiger et al. 2007) support the notion that a thermodynamic approach has validity and can be used to provide a useful 'reference frame' with which transport considerations can be contemplated. Development of an open system magmatic system model that simultaneously incorporates transport phenomena at macroscopic to molecular scales and embraces the assumption of local thermodynamic equilibrium, when appropriate and valid for three-dimensional representations, lies in the future.

The thermodynamic solutions provided by MCS are dependent on the quality of the thermodynamic data that underpins rhyolite- or pMELTS. These data include the standard state properties of all phases, activity-composition relations for all crystalline solutions defined by end-members with known standard state properties, the mixing properties of H_2O-CO_2 supercritical fluids, the form of the equation of state, and the Gibbs excess free energy model for silicate liquids. The latter gives the excess Gibbs energy of silicate melt as a function of composition, temperature, and pressure for multicomponent silicate melt. Any thermodynamic model is no better than the data and basic assumptions upon which it is based. The MELTS thermodynamic database, while robust, has its limitations. For example, the activity-composition relations for garnet, trioctahedral mica, and amphibole family phases are reasonable but imperfect. Hence, in volcanic and plutonic rocks where these phases are modally abundant, the predictions of system evolution are more uncertain. The coverage in p–T space for which the rhyolite- and pMELTS engines are optimized is roughly 1000–2000 K and 0–3 GPa, limiting modeling to the outer ~ 100 km of Earth and deeper on smaller bodies such as the Moon, Mars, Venus, Mercury and the asteroids. Fortunately, this coverage is sufficient for a great variety of igneous environments that may be modeled with MCS.

Finally, we list additional design features that are critical for the MCS user to appreciate: (1) MCS is an isobaric model, and therefore, the composite system is defined by a single pressure (e.g., Table 1); (2) during assimilation, anatectic melt is transferred between wallrock and M melt. A fluid phase and solids are not; they remain as a part of the wallrock subsystem; (3) the criterion that a threshold fraction of melt be attained in wallrock before partial melt is added to and equilibrated with resident melt is informed by the rheological properties of crystal–liquid mixtures (Lesher and Spera 2015); however, the mass of partial melt added from wallrock is simply the difference between the evolving local melt fraction in wallrock and this user-defined threshold value. There is no Darcy percolation per se. Transport details justifying melt extraction dynamics are given elsewhere (Spera and Bohrson

2001; Bohrson et al. 2014); (4) wallrock temperature is uniform throughout the entire wallrock mass; (5) the output of MCS includes mass, thermal, and compositional information for melt, solids and fluid phase for all subsystems; the user must be astute when comparing (e.g.,) melt compositions in MCS with whole-rock compositions from an igneous suite, as magmas (and their solidified equivalents) can be complex combinations of melt, crystals and fluid phase.

A complete description of the MCS along with the code (both PC and Mac versions), examples, tutorials, and related tools may be found at https://mcs.geol.ucsb.edu, the MCS website. One of the related tools, the MCS Visualizer, operates on the output produced by the MCS-PhaseEQ code to generate an animated portrayal of a simulation, and the Cumulate Calculator compiles the compositional information of the incremental and bulk cumulate and residual wallrock composition for any MCS simulation; the Cumulate Calculator is particularly useful to track compositional model data relevant to intrusive environments. The Visualizer and Cumulate Calculator are not described here; details may be found on the MCS website. The MCS is continuously being developed so the reader is referred to the website for news and the most up-to-date version available.

Comparison of Closed (Fractional Crystallization) and Open-System Magma Evolution Illustrated by MCS

We present five MCS-PhaseEQ simulations that compare the melt composition and phase equilibria evolution of a magma body undergoing fractional crystallization (FC), recharge (two events)–fractional crystallization (R_2FC), assimilation–fractional crystallization (AFC), fractional crystallization accompanied by assimilation through stoping (two events) (S_2FC), and recharge (two events)–assimilation–fractional crystallization (R_2AFC). We provide detailed comparisons of temperatures, masses, and compositions of the results, and we acknowledge that these models are illustrative; they are not intended to represent a particular magmatic system, and different parameters and starting bulk compositions will, indeed, yield different results. By presenting these cases, our intent is, first, to highlight the rich data sets that can be generated by MCS. Second, by describing the results in some detail, we hope to provide a roadmap for how MCS results can be used to unravel the RASFC evolution of a particular magmatic system. Table 3 lists MCS variables and typical ranges used in modeling of crustal systems. It also provides examples of petrological and geochemical data that can be used to both inform choice of input and to evaluate how MCS output can be utilized to determine 'best-fit' results. Finally, via these specific models, we elucidate characteristics of magma systems that may—or may not—allow identification of a specific process like crustal assimilation or magma recharge/mixing. A related longer term goal is to use MCS, in a vastly expanded way, to develop a systematic framework for identifying and distinguishing magma processes such as recharge, crustal assimilation, and crystallization.

Table 3. Typical input ranges of MCS parameters, constraints provided by plutonic and volcanic data, and guidelines for evaluating model results

MCS parameter	Typical range employed in MCS for crustal magmatic systems	Constraints provided by data from plutonic and volcanic systems	Best-fit decision making: how do I evaluate the model parameter?
Pressure of crustal magma systems	< 0.1 to ~ 1.0 GPa	Pressure-dependent phase assemblage, independent geobarometry	Different pressure runs may yield different major and trace element trends, cumulate assemblages, cumulate mineral compositions, sequence ('arrow of time') of cumulate mineral compositions
Oxygen fugacity of system	Unconstrained, IW, COH, QFM, NNO HM	Mineral equilibria. For many systems without such constraints QFM or NNO buffer is appropriate; otherwise setting at QFM to determine ferrous/ferric in M parent melt and then running unconstrained is also appropriate	Different buffers may show different major and trace element trends; typically, FeO, Fe_2O_3, TiO_2 are most distinctive; different cumulate mineral assemblages may result from different fO_2 as well
fmZero (residual melt fraction held in wallrock)	0.04 to > 0.12	Melt inclusions may provide composition of partial melt. Melt wets silicate and oxide grain boundaries to form interconnected network at low melt fractions; values at larger end of range for more silicic wallrock	Different fmZero will lead to different anatectic melt compositions, may yield different major and trace element trends, cumulate assemblages, cumulate mineral compositions. Melt inclusions may represent anatectic melt, comparison between model output and these data may help constrain fmZero
Parent magma composition	Basalt to rhyolite	Most primitive of exposed suite of related rocks, estimate of parent magma based on melt inclusions, reconstruction of parental from mineral data	Comparison of most primitive sample with initial composition of MCS run

Wallrock composition	Peridotite to granite	Outcrops, drill cores, xenoliths, melt inclusions, seismic data	Different wallrock compositions may yield different major/trace element/isotope trends, cumulate assemblages, cumulate mineral compositions, sequence ('arrow of time') of cumulate mineral compositions, in situ isotopic record
Initial wallrock temperature	0 to ~ 750 °C	Pressure estimates coupled with estimates of geothermal gradient, evidence of thermal priming	Different wallrock temperatures may yield different major/trace element/isotope trends, cumulate assemblages, cumulate mineral compositions, sequence ('arrow of time') of cumulate mineral compositions/isotopes. Will also change temperature of magma at which assimilation begins; this record may be detected in compositional and isotopic data in cumulate crystals, and via changes in isotopes in samples where absolute or relative ages are documented
Ratio of initial wallrock mass to initial magma mass	> 0 to ~ 3	Upper limit from enthalpy balance. For natural systems, the value depends on many transport and thermophysical properties as well as the state of stress in wallrock (both 'tectonic' stress and thermal stress); each natural system requires unique characterization	Different ratio may yield different major/trace element/isotope trends, cumulate assemblages, cumulate mineral compositions, sequence ('arrow of time') of cumulate mineral compositions/isotopes. Will also change temperature of magma at which assimilation begins; this record may be detected in compositional and isotopic data in cumulate crystals, and via changes in isotopes in samples where absolute or relative ages are documented

Recharge magma composition	Basalt to rhyolite	Reconstructions based on compositional zoning of crystals in solidified products, composition of enclaves, end-member composition of distinct members of mingled rocks, composition of melt inclusions	Different compositions may yield different major/trace element/isotope trends, cumulate assemblages, cumulate mineral compositions, sequence ('arrow of time') of cumulate mineral compositions/isotopes
Temperature of magma when recharge/stoping event occurs ('trigger temperature')	Liquidus temperature to near solidus temperature	Geothermometry applied to zoned crystals, to melt inclusions, and to mingled rocks, eruption temperature	Different compositions may yield different major/trace element/isotope trends, cumulate assemblages, cumulate mineral compositions, sequence ('arrow of time') of cumulate mineral compositions/isotopes. First evidence of recharge also dependent on 'trigger' temperature. Record may be detected via in situ compositional and isotopic data in cumulate crystals, and may also be detected through changes in isotopes in samples where absolute or relative ages are documented
Temperature and crystallinity ("state') of recharge magma at recharge event	Liquidus temperature to below solidus temperature, 100% melt to solid	Character of enclaves (i.e., crystal versus glass/groundmass), crystal populations in solidified products that might inform state of recharge magma	Different 'state' may yield different major/trace element/isotope trends, cumulate assemblages, cumulate mineral compositions, sequence ('arrow of time') of cumulate mineral compositions/isotopes. 'State' also impacts M melt temperature change when recharge occurs; this may be documented via geothermometry of cumulate crystals

Ratio of recharge mass to initial magma mass	< 0.1 to > 2	Compositional contrasts documented in rock suites that have relative or absolute age information (e.g., dacitic eruption followed by basaltic eruption), composition of enclaves, melt inclusions	Different ratio may yield different major/trace element/isotope trends, cumulate assemblages, cumulate mineral compositions, sequence ('arrow of time') of cumulate mineral compositions/isotopes
Temperature and crystallinity ('state') of stoped wallrock at stoping event	Near to below solidus temperature	Xenoliths or xenocrysts of crustal origin, melt inclusions	Different 'state' may yield different major/trace element/isotope trends, cumulate assemblages, cumulate mineral compositions, sequence ('arrow of time') of cumulate mineral compositions/isotopes. 'State' also impacts *M* melt temperature change when stoping occurs; this may be documented via geothermometry of cumulate crystals
Ratio of stoped block(s) mass to initial magma mass	< 1	Compositional and isotopic contrasts documented in rock suites that have relative or absolute age information	Different ratio may yield different major/trace element/isotope trends, cumulate assemblages, cumulate mineral compositions, sequence ('arrow of time') of cumulate mineral compositions/isotopes

For each simulation, the fixed composite system pressure is 0.1 GPa, which corresponds to the shallow crust at circa 3 km depth. The percolation threshold (fmZero) is 0.1 (mass fraction), which means that before anatectic melt can be transferred from wallrock to M melt, 10 wt.% melt must be present in wallrock; any mass above this threshold is transferred and equilibrated with M melt. For all simulations, the mass of wallrock involved is twice (200 mass units, m.u.) that of the initial magma (100 m.u.), yielding a wallrock/initial resident magma mass ratio of two. This choice of mass ratio implies that the heat available from the cooling and crystallization of M magma is allowed to thermally interact with country rock mass twice that of the original magma. Because the enthalpy generated by the crystallization of ferromagnesian phases (olivine, clinopyroxene, spinel) in mafic magma is higher by about a factor of two than the fusion enthalpy of the salic phases in the wallrock and because the specific isobaric heat capacity increases with increasing temperature, a mass ratio of two is justified. However, it is important to note that in MCS, the ratio of wallrock to magma is an initial parameter of the calculation. The MCS is not a heat transport model. All simulations discussed

here utilized rhyolite-MELTS v1.2.0. Tables 1, 2 list compositions and other initial conditions for the five simulations.

The parental magma for the five simulations is depleted mantle-derived continental tholeiite from the ~ 180 Ma Karoo Large Igneous Province (sample P27-AVL, Luttinen and Furnes 2000) (Table 1). Initial H_2O was set at ~ 2 wt.%, and the Fe^{2+} to Fe^{3+} ratio was initially calculated at FMQ (at liquidus temperature of 1129 °C and pressure of 0.1 GPa); each simulation was then run under fO_2-buffer absent conditions. This means that the system is closed with respect to the addition or subtraction of oxygen, and thus, during the run, the fugacity of oxygen will rise or fall according to the dictates of Gibbs energy minimization of the composite system. Each simulation has a user-chosen magma temperature decrement of 5 °C, which means that the state of the system (magma and wallrock melt, minerals, fluid phase) is determined and archived at 5 °C temperature decrements for the FC case (Table 2). Within these 5-degree decrements, the M subsystem can be envisaged to evolve by equilibrium crystallization after which the formed minerals are fractionated to the cumulate pile before the next step. MCS-PhaseEQ internally adjusts the M melt and cumulate temperature to values other than those defined by the user-defined decrement in response to the homogenization of recharge magma(s), stoped block(s), or anatectic melt with M melt.

For the cases involving recharge (i.e., R_2FC, R_2AFC), the recharge magma compositions (including initial H_2O wt.% and fO_2) are identical to parent (resident) magma. Wallrock bulk composition is average upper continental crust from Rudnick and Gao (2003), with initial fO_2 calculated at FMQ (at 740°C and 0.1 GPa), initial H_2O of ~2 wt.%, and initial CO_2 of ~1 wt.% (Table 1).

The models are discussed and compared in detail below. Online Resource 1 provides input for the cases (similar to Table 1 but in Excel format), and Online Resources 2–5 present detailed comparison data for mass and temperature outcomes, mineral assemblage, fluid saturation, and selected melt compositional parameters for resident magma, wallrock, and recharge magmas for each case. Figure 2 shows the model outcomes in illustrations that are annotated snapshots from the MCS Visualizer tool and Figs. 3, 4, 5, 6, 7, 8 illustrate selected mass, thermal, and compositional data for melt and minerals for resident magma and wallrock.

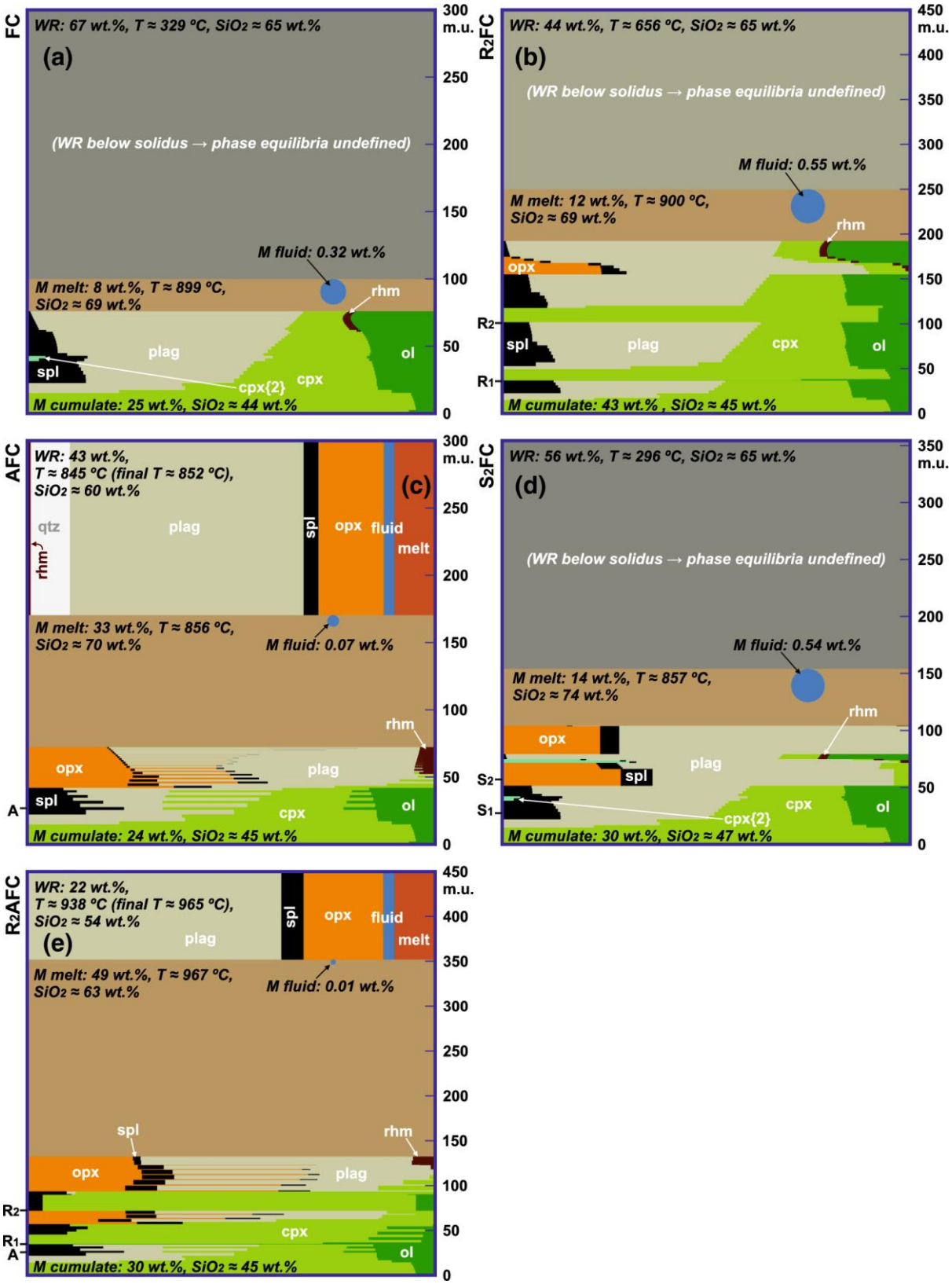

Figure 2. Results of MCS-PhaseEQ simulations for five cases (FC, AFC, R_2FC, S_2FC, R_2AFC) shown in annotated MCS Visualizer snapshots that depict the situation after the final magma crystallization step (AFC and R_2AFC include one additional step of wallrock equilibration before the simulation ends). Completions of R and S events and beginning of A are indicated in the cumulate pile where applicable. Note that the phase

proportions are based on mass fractions not volume fractions and that the wt.% of the subsystems are relative to the whole magma-wallrock system; M melt, M fluid, and M cumulate comprise the total magma chamber mass. See Online Resource 8 for full animations. Mineral abbreviations: *ol* olivine, *opx* orthopyroxene, *cpx* clinopyroxene (FC and S_2FC include two separately output cpx solid-solution phases, see the respective outputs in Online Resource 6), *plag* plagioclase, *qtz* quartz, *spl* spinel, *rhm* rhombohedral oxide.

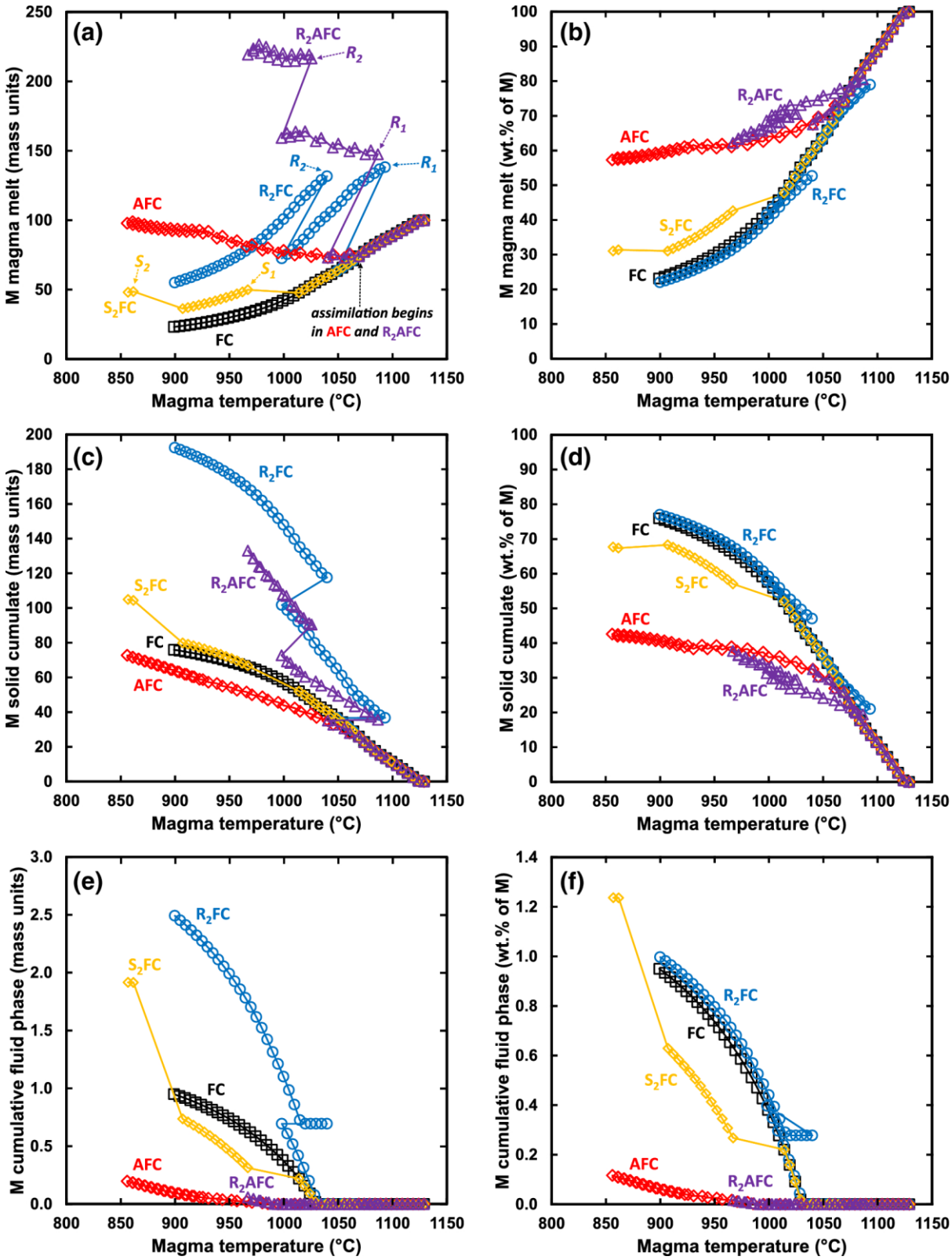

Figure 3. Results of MCS-PhaseEQ simulations for five cases (FC, AFC, R_2FC, S_2FC, R_2AFC) shown in magma temperature (°C) versus **a** absolute and **b** relative M magma liquid (melt) mass, **c** absolute and **d** relative total cumulative mass of crystals removed to the cumulate reservoir, and **e** absolute and **f** relative total cumulative mass of fluid phase. Each simulation runs from parent magma liquidus temperature to the end of the simulation. For cases involving assimilation, the simulation ends when magma and wallrock are at or close to

thermal equilibrium. For cases that do not involve assimilation, the simulation ends at a user-defined "hard stop" temperature. Completions of R and S events and beginning of A are indicated for the relevant runs in a. See text, tables and Online Resources for additional details.

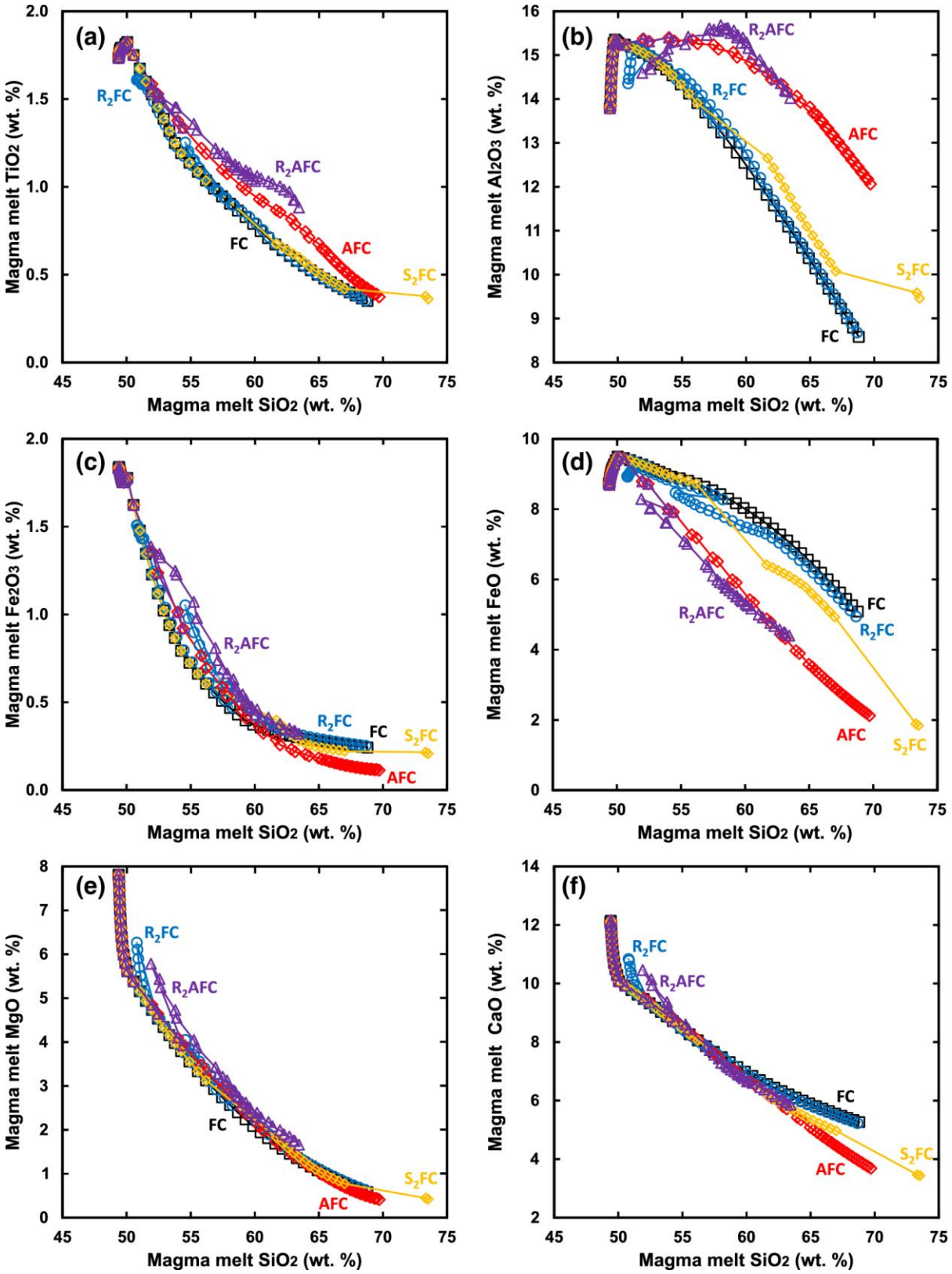

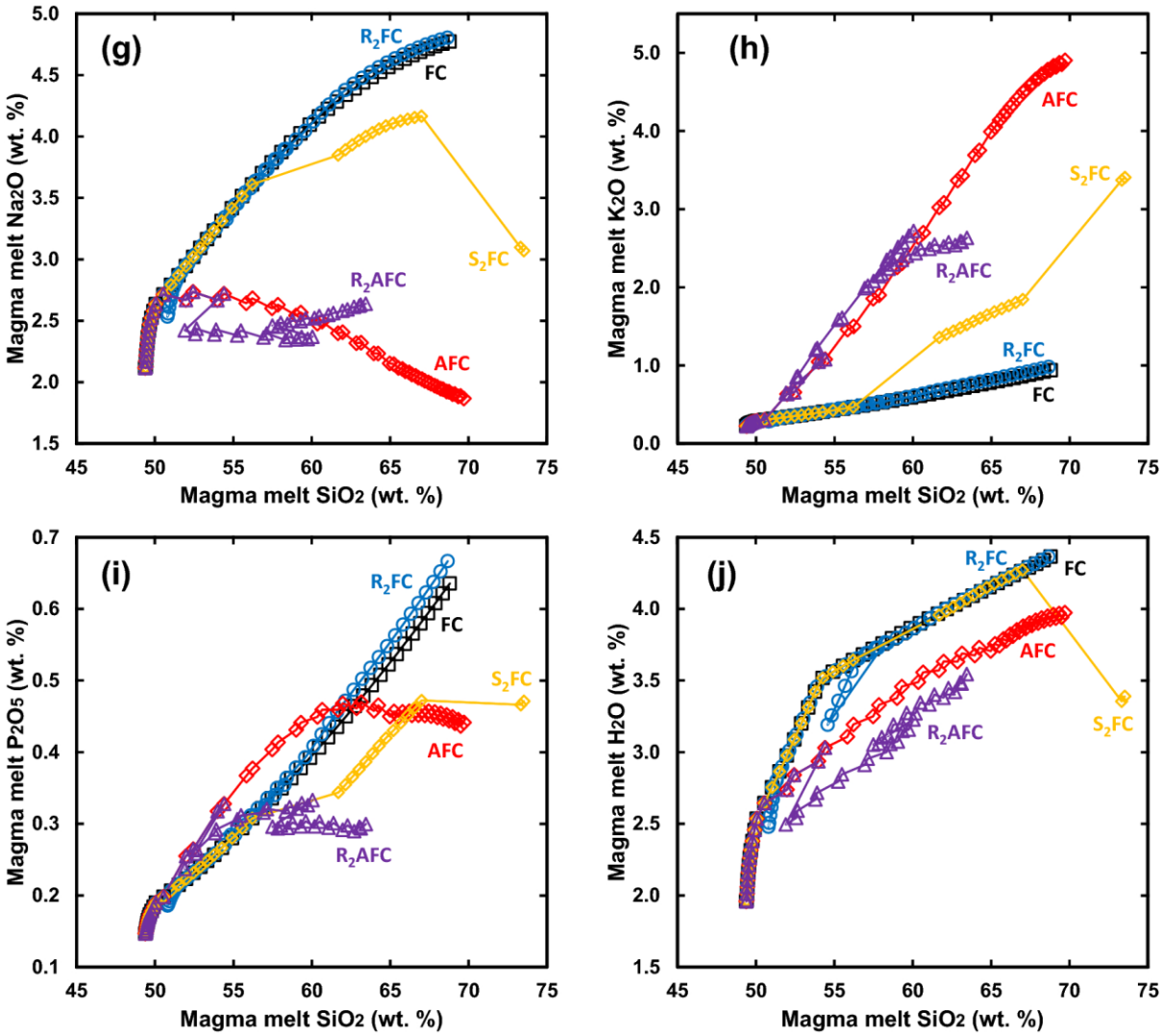

Figure 4. Results of MCS simulations for five cases (FC, AFC, R_2FC, S_2FC, R_2AFC) shown in magma melt SiO_2 (wt.%) versus **a** TiO_2, **b** Al_2O_3, **c** Fe_2O_3, **d** FeO, **e** MgO, **f** CaO, **g** Na_2O, **h** K_2O, **i** P_2O_5, and **j** H_2O (wt.%).

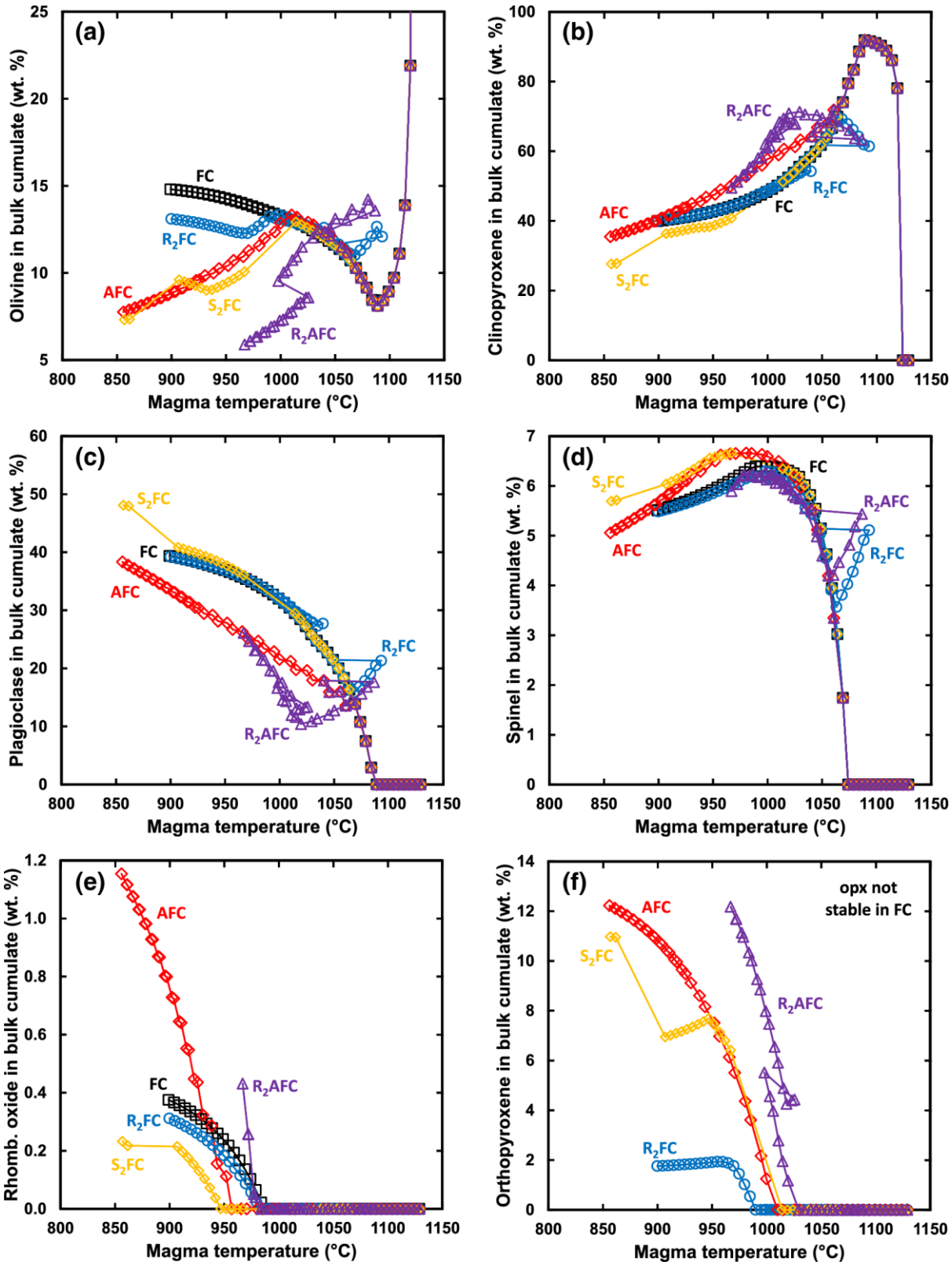

Figure 5. Magma temperature (°C) versus wt.% of minerals in the bulk cumulate in the five MCS simulations. **a** olivine, **b** clinopyroxene (cpx), **c** plagioclase, **d** spinel, **e** rhombohedral oxide, and **f** orthopyroxene (opx).

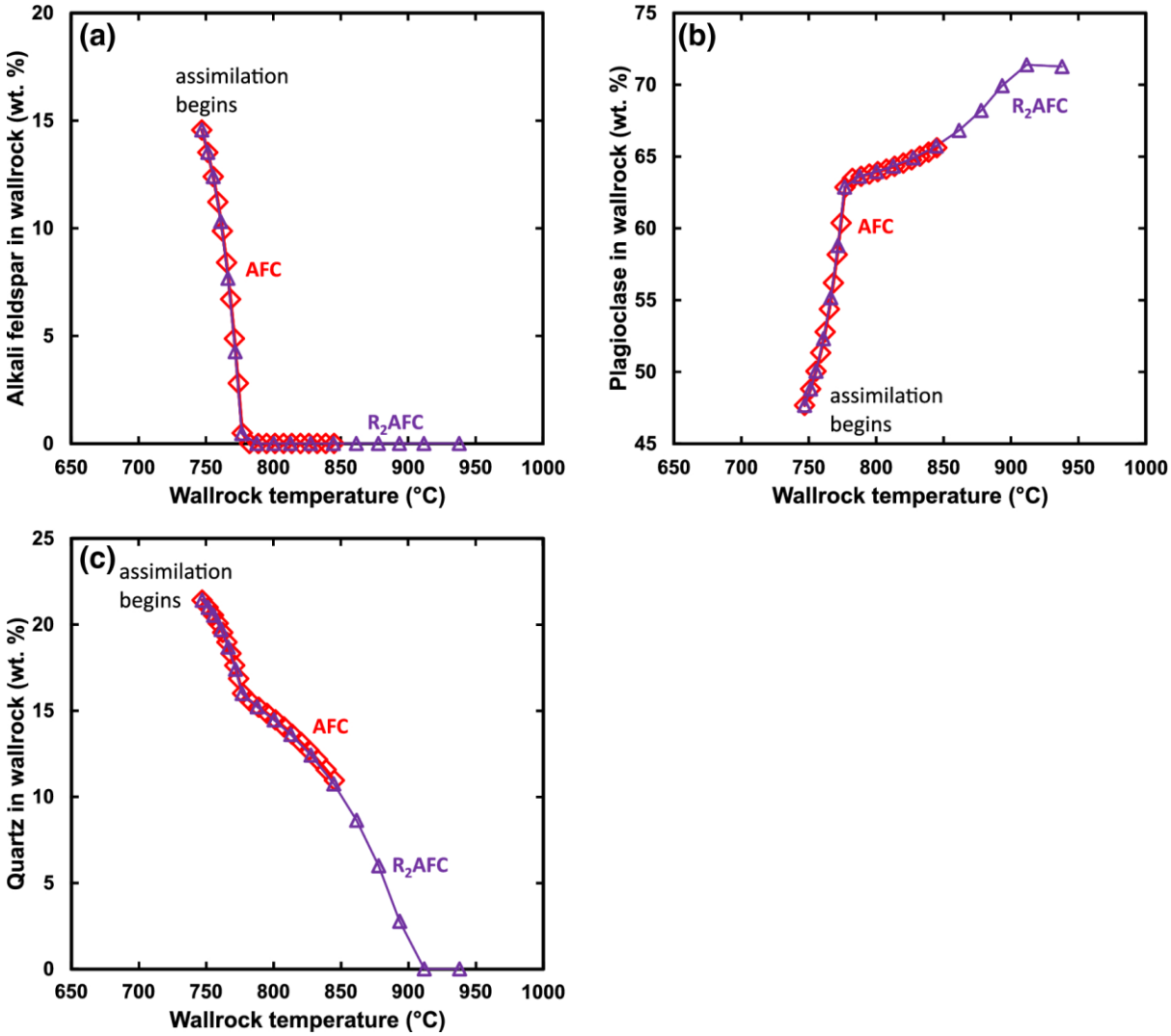

Figure 6. Wallrock temperature (°C) versus wt.% of **a** alkali feldspar, **b** plagioclase, and **c** quartz in wallrock solids (restite after partial melt is transferred to magma) for two MCS cases involving assimilation of wallrock anatectic melt (AFC, R_2AFC). Wallrock initial temperature is 700 °C, and assimilation starts at wallrock temperature of 747 °C when the percolation threshold has been exceeded. Wallrock heats up to the end of the simulation, where magma and wallrock temperature are at or close to thermal equilibrium.

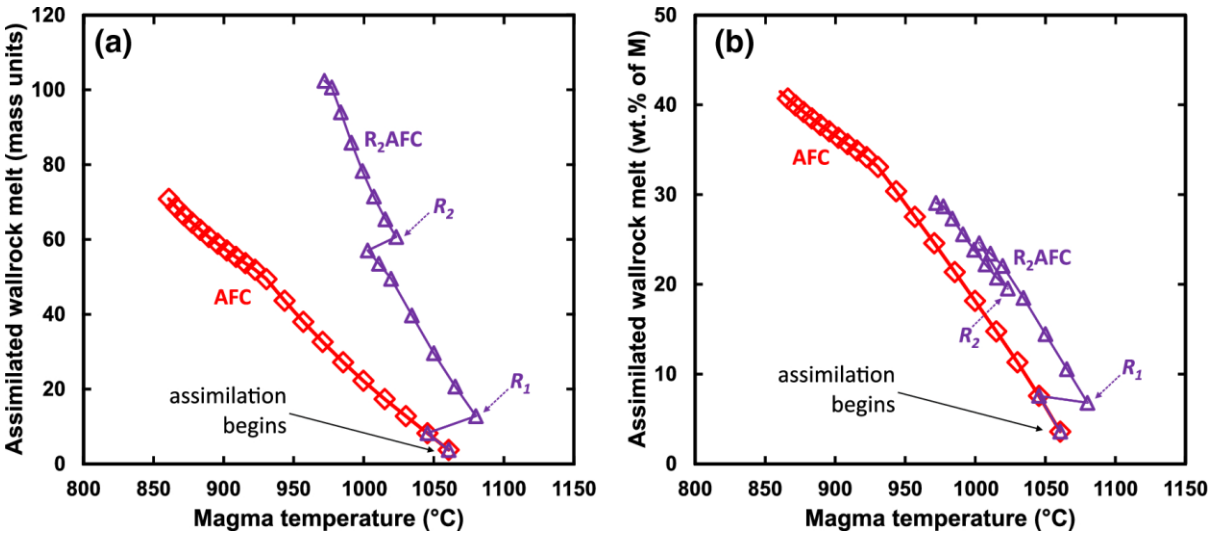

Figure 7. Magma temperature (°C) versus **a** absolute and **b** relative amount of cumulative anatectic melt assimilated into M melt once assimilation begins. Completions of the R events for the R_2AFC case are indicated.

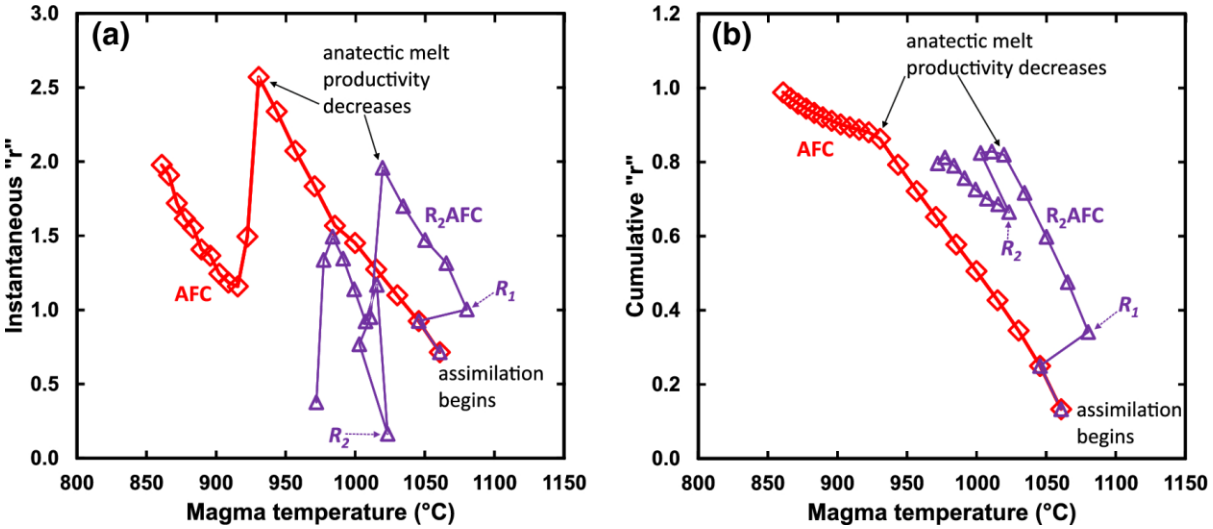

Figure 8. Magma temperature (°C) versus **a** instantaneous "*r*", and **b** cumulative "*r*" shown for two MCS cases with assimilation of wallrock anatectic melt (AFC, R_2AFC). The definition of "*r*" is based on DePaolo (1981) and is the mass of anatectic melt assimilated/mass of crystals formed. Instantaneous refers to those masses for each individual temperature step where assimilation ± recharge occurs, and cumulative refers to the total mass of anatectic melt assimilated/total mass of cumulates produced from the start of the simulation to the magma temperature shown. The value of "*r*" is zero before assimilation begins, and for simplicity, this part of the AFC or R_2AFC is not shown. Instantaneous and cumulative "*r*" after completion of recharge events 1 and 2 labeled, as are the values at which anatectic melt productivity decreases due to complete reaction of alkali feldspar. See text for discussion.

All model input and output are presented in Online Resource 6, and we recommend viewing the output files (concentrating on the RunSummary tab) simultaneously when reading the following sections. The structure of the output files is uniform across all cases and, hence, time invested in learning the structure of the output makes the digestion of data relatively easy after an investment of effort. By way of introduction, the different tabs of the output that store the relevant information are specifically named in the discussion of the FC case. In addition, the MES input files are included in Online Resource 7; this means that all the cases discussed here can be replicated. It should be noted that there can be small differences at the part per thousand level when MCS is run in different computing environments. These differences are well below levels that have an impact on interpretation of results in cases where we have studied this phenomenon. Finally, case-specific animations that help to follow the changes in the bulk system and which were built with the MCS Visualizer are given in Online Resource 8.

Case 1: Fractional Crystallization (FC)

The output of the FC case is stored in "MCS-FC_output_PhaseEQ.xlsx" file in Online Resource 6. The parent basalt specified above has a liquidus temperature of ~ 1129 °C at 0.1 GPa, and the FC simulation ends at a user-chosen temperature of ~ 900 °C. Via fractional crystallization, the melt composition evolves from tholeiitic basalt to dacite, with the dacitic melt forming through ~ 76 wt.% fractional crystallization (Figs. 2a and 3, see ChartTAS tab in the output). Magma melt becomes H_2O-saturated at ~ 1029 °C. At the end-temperature (~ 900 °C), the H_2O-fluid phase constitutes ~ 1 wt.% of the magma system, with melt composing the remaining ~ 23 wt.% (Fig. 3) as noted by examination of columns *I* through *L* on row 52 of the RunSummary tab in the output. Major oxide trends behave as anticipated for a basaltic system undergoing fractional crystallization (Fig. 4).

Olivine is the first liquidus phase (see column *Z* of the RunSummary tab), and its composition is Fo_{82} (line 269, SolidFormulas tab, color code darker blue). It is followed closely by clinopyroxene (first appearance at ~ 1119 °C) and plagioclase (first appearance at ~ 1084 °C, An_{84}). Additional phases include spinel (first appearance at ~ 1069 °C) and rhombohedral oxide (first appearance at ~ 984 °C). By the end of crystallization, the cumulate is dominated by clinopyroxene and plagioclase, each of which composes ~ 40 wt.% of the bulk cumulate mass; olivine constitutes ~ 15 wt.%, spinel ~ 6 wt.% and rhombohedral oxide < 1 wt.% (Fig. 5). This information is graphically portrayed on the output tabs ChartMassFrac, ChartPPD, and ChartPMD. The compositional range of minerals is large (see output SolidFormulas tab and Online Resource 3), as anticipated for a parental basaltic melt that evolves to dacitic after significant fractional crystallization.

The initial wallrock temperature for this simulation is 100 °C. Enthalpy transferred from magma due to cooling and crystallization yields a final wallrock temperature of ~ 329 °C (Fig. 2a), too low for

any partial melting to occur. Thus, although the wallrock heats up, it remains below its solidus temperature, and no mass transfer occurs.

Case 2: Recharge-Fractional Crystallization (R_2FC)

The output of the R_2FC case is stored in "MCS-R2FC_output_PhaseEQ.xlsx" file in Online Resource 6. Two recharge events simulate intrusion of mantle-derived magma into resident magma melt as it evolves by fractional crystallization in an upper crustal (0.1 GPa) magma storage system. The first recharge event involves a recharge magma/initial magma mass ratio of 0.75 (that is, for an initial parent melt mass of 100 m.u., 75 m.u. of recharge magma is added (Table 2)). This recharge magma at ~ 1130 °C (100 wt.% melt) intrudes into and fully hybridizes with resident melt at ~ 1049 °C (Tables 1, 2, Online Resource 2). Note that the temperature at which recharge actually occurs differs slightly from that reported in the input (Table 2, 1050 °C), because the recharge event occurs in the step after the target temperature is reached. Prior to the first recharge event, the resident magma had been crystallizing a mineral assemblage of olivine (Fo_{70}) + clinopyroxene ($Mg\#_{77}$) + plagioclase (An_{81}) + spinel. Immediately following the recharge event, the new, equilibrated state of hybridized M melt yields a new temperature of 1093 °C due to addition of enthalpy from recharge magma, and crystallization of clinopyroxene, plagioclase, and spinel is suppressed. Thus, in response to mixing, resident magma (melt + cumulates) temperature increases by almost 50 °C and the hybridized magma crystallizes only olivine that is more magnesian (Fo_{78}) than olivine crystallizing just prior to the recharge event. With 5 °C of additional post-recharge cooling, clinopyroxene ($Mg\#_{82}$) returns to the M crystallizing assemblage, and with an additional ~ 25–30 °C of cooling, plagioclase (An_{82}) and spinel also returns to the crystallizing assemblage. For most major oxides, the first recharge event has only a subtle effect on resident melt composition: the most pronounced changes are an increase in MgO from ~ 4.4 to 6.2 wt.%, and a decrease in SiO_2 from 52.6 to 50.9 wt.% (Fig. 4).

The second recharge event is compositionally identical to and has the same mass constraints as the first (75 m.u.), but for this recharge event, the temperature of the recharge magma is ~ 1080 °C; thus the magma is 21 wt.% crystalline [mode of the assemblage is ~ 12 wt.% is olivine (Fo_{76}), ~ 82 wt.% is clinopyroxene ($Mg\#_{81}$), and ~ 6 wt.% is plagioclase (An_{83})] at the time recharge is triggered (Online Resource 5). This second "event" yields a new M temperature of ~ 1040 °C, an increase of ~ 40 °C. Plagioclase and spinel crystallization is suppressed for only ~ 5 °C. The compositions of the minerals change in response to recharge: olivine ($Fo_{55} \rightarrow Fo_{68}$) + clinopyroxene ($Mg\#_{70} \rightarrow Mg\#_{77}$) + plagioclase ($An_{71} \rightarrow An_{77}$). At 985 °C, orthopyroxene joins the mineral assemblage, followed by rhombohedral oxide at ~ 980 °C; orthopyroxene crystallization ceases at 955 °C. Importantly, some of the major oxide changes pre- and post-recharge are more profound compared to the first recharge event, because the contrast between resident melt and recharge magma

is greater. For example, from pre- to post-recharge, SiO_2 decreases from ~ 58 to 54.5 wt.% (as opposed to a decrease of < 2 wt.% SiO_2 in M following Recharge event 1; see also Fig. 4).

The final temperature of the R_2FC simulation is ~ 900 °C, and the final melt composition is dacitic. The final R_2FC melt major oxide compositions are similar to those of the FC case; that is, the record of the increases in MgO and decreases in SiO_2 is not preserved in the final melt composition (Fig. 4), although a record is preserved in the compositional record of the cumulate phases. The proportion of crystals, melt, and fluid phase at the final simulation temperature is similar between R_2FC and FC (~ 77 wt.% crystals, 22 wt.% melt, 1 wt.% fluid for R_2FC versus ~ 76 wt.% crystals, 23 wt.% melt, 1 wt.% fluid for FC, respectively; Fig. 3). The proportions of phases in the final cumulate are similar, with the obvious exception of orthopyroxene, which makes up ~ 2 wt.% of the final cumulate in R_2FC (Fig. 5). The general range of mineral compositions is also similar (Online Resource 3).

What is distinctly different between FC and R_2FC is the overall mass of the system, which is ~ 2.5 times greater in R_2FC, because the recharge events add 150 (2 × 75) m.u. into the system. Thus, the total mass of the R_2FC system is 250 m.u., compared to 100 m.u. in the FC case. The masses of melt, cumulates, and fluid are also proportionally larger, as anticipated (Fig. 3). Finally, the larger magma system mass significantly affects the wallrock temperature, with a final wallrock temperature of ~ 656 °C, compared to ~ 329 °C for FC alone (Fig. 2). The hotter wallrock is due to the added enthalpy of recharge magma intruding into resident melt. This suggests that recharge systems are more prone to induce partial melting in their host rocks due to this 'enthalpy-pumping' effect (all other conditions remaining constant).

Case 3: Assimilation-Fractional Crystallization (AFC)

The output of the AFC case is stored in "MCS-AFC_output_PhaseEQ.xlsx" file in Online Resource 6. This case reflects assimilation of upper continental crust by a depleted continental tholeiite evolving in an upper crustal (0.1 GPa) magma storage system. All other parameters being identical, the initial conditions of the AFC simulation contrast with those of the FC case with regard to the initial temperature of wallrock; it is 700 °C compared to 100 °C. The elevated wallrock temperature is intended to maximize the assimilation signature and simulates assimilation in crust that has been thermally primed by previous episodes of magmatism (e.g., Moore et al. 2018).

As resident melt cools from its liquidus, it first evolves like in the FC case. For a wallrock/initial magma mass ratio of two, anatectic (wallrock) partial melt begins to contaminate magma melt at a M melt temperature of ~ 1069 °C (Fig. 3a). At this point, the wallrock is ~ 747 °C and its percolation threshold (10 wt.%) for anatectic melt has been exceeded. Anatectic melt above this limit is transferred into, and thoroughly hybridized and equilibrated with M melt. Note that because incoming

anatectic melt is at a lower temperature and different specific enthalpy than M melt, the assimilation of wallrock partial melts drives M melt to a slightly lower temperature. This is a consequence of the isenthalpic AFC process. That is, the energy for partial melting of wallrock is derived by the cooling and crystallization of the M subsystem. The new, lower magma temperature following assimilation can catalyze crystallization of the contaminated melt. These crystals, like all crystals in MCS-PhaseEQ, become part of the cumulate reservoir, where they remain in thermal contact with M melt.

At the onset of assimilation, the assemblage that crystallizes continues to be olivine + clinopyroxene + plagioclase + spinel, albeit in slightly smaller proportions than before AFC onset. Contaminated melt becomes fluid saturated at ~ 985 °C, which is ~ 44 °C lower than the FC case; this is most likely due to the design feature in MCS that does not (currently) permit fluid phase transfer with anatectic melt, although H_2O does enter into M magma, because anatectic melt is H_2O-saturated. This effect is mediated by pressure. At the low pressure of the simulation, the water-content of anatectic melt is low since the solubility of water in anatectic melt is small. At higher pressure, more H_2O component would be delivered to M magma by partial melt assimilation. At magma temperature ~ 1000 °C, olivine becomes unstable, and is replaced by orthopyroxene. At ~ 952 °C, rhombohedral oxide joins the stable mineral assemblage and clinopyroxene crystallization effectively ceases (Fig. 5).

By the terminus of the run (M-WR equilibration temperature of ~852°C), contaminated M melt has evolved to a dacitic composition; at that temperature, the final wt.% SiO_2 produced by the FC and AFC runs are within 1 wt.% (69 versus 70 wt. %, Fig. 4) of each other. Once assimilation begins, at the same SiO_2 compared to FC, AFC Al_2O_3 and K_2O have distinctly higher concentrations, whereas Na_2O, H_2O, and FeO are lower. CaO, MgO, Fe_2O_3, and TiO_2 are similar, and P_2O_5 behavior is more complicated: it is initially a bit higher and then distinctly lower at the same SiO_2 (Fig. 4).

The effect of assimilation on crystallization is marked; the proportion of crystals in the cumulate reservoir of the AFC magma system (~ 43 wt.%) is much smaller than that associated with FC (76 wt.%); the proportion of fluid phase in AFC is an order of magnitude smaller (0.1 versus 1 wt.%) (Fig. 3). The final AFC cumulate is different than the FC one; there is slightly less olivine and clinopyroxene, very similar percentage of plagioclase, and in AFC, orthopyroxene makes up ~ 12 wt.% of the final cumulate (Fig. 5). In addition, the total ranges in olivine and plagioclase compositions are different (Online Resource 3). The last olivine to crystallize in AFC is Fo_{62} (compared to Fo_{23} in FC) and the final plagioclase to crystallize is slightly more anorthitic (An_{54}) compared to FC (An_{47}). Thus, addition of anatectic melt changes not only the crystallizing assemblage (e.g., orthopyroxene precipitates, and olivine and clinopyroxene disappear as cumulus phases) but also changes the balance of melt versus cumulate (Fig. 3). AFC also delays the onset of fluid saturation by tens of degrees, and the total proportion of the magma system that is an exsolved fluid phase is much smaller (Fig. 2c).

The mineral abundances of wallrock at its solidus are plagioclase > > quartz > alkali feldspar > orthopyroxene; spinel + rhombohedral oxide + biotite + apatite are accessory phases (Online Resource 4). Note also that wallrock is fluid saturated. Wallrock reaches its percolation threshold temperature at ~ 747 °C; in the first instance of partial melting above the percolation threshold, apatite reacts and ceases to be a part of the wallrock residual mineral assemblage; the same is true of biotite. The restite assemblage of plagioclase + quartz + alkali feldspar + orthopyroxene, with accessory spinel + rhombohedral oxide, persists until wallrock temperature ~ 782 °C, at which point, alkali feldspar is totally consumed (Fig. 6a). The remaining minerals persist in wallrock restite to the equilibration temperature.

For each step of anatectic melt transfer into M melt (except the first one), the size of anatectic melt increment is ~ 2–3 wt.% of the initial mass of the wallrock system (i.e., mass transfer involves ~ 4–6 m.u. of the initial 200 m.u. of wallrock). This mass rate of melt transfer changes when alkali feldspar completely dissolves. After this (wallrock T ~ 782 °C, Fig. 6a), wallrock melt productivity decreases, and the size of the increments transferred goes down to < 1 wt.% of the initial wallrock mass (< 2 mass units) (Fig. 7, magma T ~ 920 °C where slope changes slightly). Anatectic melt that is transferred and homogenized with resident magma melt is mostly rhyolitic, varying in SiO_2 between ~ 70 (at onset of assimilation) and 76 wt.% (at the equilibration temperature). The cumulative percent anatectic melt added to the magma system can be viewed in two different ways. The total proportion of the wallrock system that was assimilated into resident magma is ~ 35 wt.% (~ 71 m.u. of the initial 200 m.u., Fig. 7). When assessed as a part of the resident magma, this assimilated mass represents about 41 wt.% of the final resident magma (melt + crystals + fluid phase body mass: ~ 71 m.u. of the final 171 m.u. system). By the time thermal equilibrium is attained, the wallrock has melted ~ 42 wt.%; this value is different than the total amount of wallrock assimilated, because 10 wt.% anatectic melt remains within the wallrock system. See Online Resource 2 for details of these mass relations.

In the current available version of MCS, fluid phase present in WR is not permitted to transfer from WR to M. There may be circumstances that favor fluid phase bulk transfer with partial melt as it percolates into M magma. For example, fluid bubbles of low viscosity may be swept into M melt by the same Darcian percolative flow that transports partial melt. The likelihood of such transport depends on many factors including the bulk H_2O content of wallrock as well as the stability of possible hydrous phases such as amphibole or biotite. Work to provide the user with the ability to transfer fluid phase, when it exists in wallrock, is ongoing and will be presented in an updated version of MCS. To assess the effects of possible fluid transfer on the results presented here, four comparisons were run in which the M melt compositions at two temperatures (1061 °C and 861 °C) were adjusted by arbitrarily adding 20 wt.% and 40 wt.% of the mixed ($H_2O + CO_2$) fluid present in wallrock at the relevant temperatures (i.e., the temperature of WR in the AFC run at the M

temperatures of 1061 and 861 °C) of 747 °C and 845·°C, respectively. These new, "fluid-enhanced" magmas were examined in rhyolite-MELTS v 1.2.0 at 1055 °C and 855 °C using the equilibrium crystallization function. (i.e., 5 °C below the temperature of fluid enhancement). The phase assemblages between the MCS results and the rhyolite-MELTS results are virtually identical, as are the M melt compositions. The only significant difference is the mass/proportion of fluid phase in the melt. The likelihood that M magma fluid saturates is obviously higher when fluid phase is allowed to migrate across the wallrock-magma subsystem boundary. See Online Resource 9 for the outcomes of this comparison.

Case 4: Assimilation through Stoping-Fractional Crystallization (S_2FC)

The output of the S_2FC case is stored in "MCS-S2FC_output_PhaseEQ.xlsx" file in Online Resource 6. Stoping in MCS is considered as a process whereby crustal contamination (synonymous with crustal assimilation) occurs via reaction of a block (or a set of multiple small blocks with a combined mass equal to the respective S event) of wallrock incorporated wholesale into magma melt. The pre-stoping temperature of the stoped block dictates its thermodynamic state; that is, the block can be stoped with different proportions of crystals, melt, and fluid phase. The S_2FC case presented here involves two stoping events, with all other parameters being identical to those of the FC case.

In MCS, stoped blocks are incorporated into M melt using the recharge function since the thermodynamics of stoping are identical to those of magma recharge and mixing. The initial (bulk) composition of the stoped blocks, however, is the same as initial wallrock in the AFC case (Table 1). Stoped block temperatures and masses were chosen, where possible, to provide relevant comparison with the AFC case. For stoping event 1, the mass of the stoped block was chosen to reflect the cumulative mass of anatectic melt assimilated by M by ~ 1015 °C (~ 17 m.u.; the ratio of stoped block to initial magma mass is 0.17); the temperature of the stoped block was chosen to reflect the wallrock temperature at that point as well (~ 760 °C). At 760 °C, the (mushy) block is composed of ~ 78 wt.% crystals, 20 wt.% melt and 2 wt.% fluid phase, and its mineral assemblage is plagioclase > quartz > orthopyroxene > alkali feldspar, with spinel and rhombohedral oxide as accessory phases. The co-existing melt is rhyolitic and fluid saturated. We note that in contrast to the current version of MCS in which fluid phase is not able to transfer into M melt during partial melt assimilation, stoping allows the fluid phase to be incorporated into M melt. Prior to the first stoping event, resident magma temperature was ~ 1014 °C, and M melt was crystallizing olivine + clinopyroxene + plagioclase + spinel. Following complete homogenization of the stoped block (including its fluid phase), the resident magma temperature decreased to 967 °C, and orthopyroxene becomes stable in the cumulate assemblage over the range 967–947 °C. Rhombohedral

oxide is the final phase to join the crystallizing assemblage at a magma temperature of 942 °C. Upon stoping, resident magma melt SiO_2 increases from ~ 56 to ~ 62 wt.% (Fig. 4).

The second stoped block reflects the conditions of the wallrock in the AFC run at M temperature ~ 908 °C; at this temperature, the wallrock is ~ 795 °C and cumulative anatectic melt assimilated is ~ 55 m.u. (ratio to initial magma mass is ~ 0.55). Stoped block 2, therefore, has a temperature of ~ 795 °C and its mass is 38 m.u. (55–17 that was assimilated in the first stoping event). Stoped block 2 is hotter than stoped block 1, and therefore, it has proportionally more melt: crystal, melt, fluid phase proportions are 60, 38, and ~ 2 wt.%, respectively. Its mineral composition is plagioclase > > orthopyroxene > quartz, with accessory spinel and rhombohedral oxide. Like stoped block 1, the co-existing melt is rhyolitic and fluid saturated. For stoping event 2, the magma temperature before stoping is ~ 907 °C and after stoping is 862 °C. Prior to the second stoping event, resident magma was crystallizing olivine + clinopyroxene + plagioclase + spinel + rhombohedral oxide. Following assimilation of the second stoped block, olivine and clinopyroxene cease to crystallize, and orthopyroxene becomes a part of the cumulate assemblage. Upon the second stoping event, SiO_2 increases from ~ 67 to ~ 73 wt.% (Fig. 4).

This simulation ends at ~ 856 °C, which is a similar end temperature to that of the AFC case. Compared to assimilation of anatectic melt ('classical' AFC), stoping favors crystallization, as the resultant proportion of crystals in the magma system is higher in S_2FC (68 wt.%) than AFC (43 wt.%; Fig. 3d). The percent fluid phase is also higher in S_2FC (Fig. 3e). The final cumulate shares some characteristics with those of the AFC case: similar percentages of olivine, spinel, and orthopyroxene, slightly less clinopyroxene and less rhombohedral oxide, and slightly more plagioclase (Fig. 5). The range of olivine composition is more similar to the FC case. Interestingly, plagioclase in S_2FC is the most albitic of all the simulations (Online Resource 3). The final melt at ~ 856 °C is rhyolitic. Oxide concentrations are more similar to the FC case than the AFC case (Fig. 4). For example, the distinct enrichment in Al_2O_3 seen in the AFC case is absent in the stoping case. K_2O is enriched compared to FC, but less so than AFC.

The final temperature of wallrock is 296 °C. This is the lowest final wallrock temperature of the five simulations. Adding cooler stoped bocks impacts the amount of enthalpy available for wallrock heating. In addition, upon stoping, in the new equilibrium M melt, quartz and alkali feldspar (where present in the stoped block) are not stable. Hence, there is an enthalpy cost to resorbing/reacting these phases, which decreases enthalpy available for transfer into the wallrock.

Case 5: Recharge-Assimilation Fractional Crystallization (R_2AFC)

The output of the R_2AFC case is stored in "MCS-R2AFC_output_PhaseEQ.xlsx" file in Online Resource 6. The two recharge events from the R_2FC case were imposed on the AFC case; recall that

the wallrock initial temperature is high (700 °C) and reflects an assumption that previous magma intrusion raised the wallrock temperature compared to an ambient geotherm. For the two recharge events, like R_2FC, the recharge magma/initial magma mass ratio is 0.75, and the temperatures of the recharge magmas at the instance of recharge are 1130 °C and 1080 °C for recharge events 1 and 2, respectively. Also, like R_2FC, recharge magma 1 is 100 wt.% melt, and recharge magma 2 is 21 wt.% crystalline. Assimilation begins at magma temperature of ~ 1069 °C as in the AFC run (Fig. 3a), and by recharge event 1, M has assimilated ~ 8 wt.% anatectic melt (where percent is calculated based on the initial mass of resident magma—i.e., cumulative addition of 8 m.u. of anatectic melt). Immediately preceding recharge event 1, the magma temperature is ~ 1041 °C, with a crystallizing mineral assemblage of olivine + clinopyroxene + plagioclase + spinel. In response to recharge event 1, the resident magma temperature increases to ~ 1087 °C, and plagioclase and spinel stop crystallizing. SiO_2 decreases from ~ 54 to 52 wt.% and MgO increases from 3.9 to 5.8 wt.% (Fig. 4).

After the first recharge event, AFC continues; at ~ 1050 °C, spinel rejoins the crystallizing assemblage, and at magma temperature ~ 1020 °C, orthopyroxene starts to crystallize and at ~ 1014 °C, plagioclase rejoins the crystallizing assemblage. Recharge event 2 is triggered when the resident magma is 998 °C; the addition of enthalpy via recharge heats the resident magma to ~ 1026 °C. Olivine begins to crystallize again for a small temperature interval, and plagioclase and orthopyroxene briefly stop crystallizing. After ~ 10 °C of cooling, the mineral assemblage returns to its pre-recharge assemblage of clinopyroxene + plagioclase + spinel + orthopyroxene. At 991 °C, clinopyroxene ceases to crystallize, and magma melt reaches fluid saturation (with a mixed $H_2O + CO_2$ fluid), but the proportion of fluid phase in the magma system is quite small (~ 0.001 m.u.; Fig. 3e). At 979 °C, rhombohedral oxide joins the assemblage. A modest change in melt composition is noted; upon recharge, SiO_2 again decreases, this time from ~ 60 to 57.5 wt.% and MgO increases from 2.3 to 3.2 wt.% (Fig. 4).

The equilibration temperature for R_2AFC is ~ 965 °C. The final magma melt composition is distinctly lower in SiO_2 compared to the other four simulations and plots at the low SiO_2 end of the dacitic field. R_2AFC manifests a similar enrichment in Al_2O_3 and K_2O compared to AFC; likewise, the depletions in FeO, H_2O and Na_2O are similar to AFC (Fig. 4). P_2O_5 is the least enriched among all cases. Like AFC, R_2AFC suppresses crystallization. Regardless of their high absolute mass of 133 m.u., crystals make up only ~ 38 wt.% of the magma body in the R_2AFC run, compared to ~ 76 wt.% in FC, and R_2AFC expresses the smallest degree of fluid saturation (Fig. 3). The range of olivine and plagioclase compositions is most similar to AFC, with the most Fe-rich olivine being Fo_{66} and the most Na-rich plagioclase being An_{70} (Online Resource 3).

For each step of anatectic melt transfer into magma melt, the size of anatectic melt increment is ~ 2–5 wt.% of the initial wallrock system (i.e., 4–10 m.u.) and generally increases as wallrock heats up. This changes after alkali feldspar completely reacts and ceases to be part of the wallrock solid

assemblage. After this (wallrock temperature of ~ 788 °C, magma temperature ~ 1015 °C, Fig. 7), wallrock melt productivity decreases and the size of the increments transferred decreases to 1–2 wt.% of the initial wallrock mass (3–4 m.u.). Melt productivity increases again at wallrock temperature of ~ 845 °C. Like the wallrock melt in AFC, the anatectic melt that is transferred and homogenized with resident magma melt is mostly rhyolitic (~ 70–76 SiO_2).

At the equilibration temperature of ~ 965 °C, ~ 51 wt.% of the wallrock system has been assimilated into the resident magma (102 m.u. out of the original 200; Fig. 7a). Thus, substantially more anatectic melt was assimilated due to recharge, consistent with more enthalpy being available from magma cooling and crystallization to heat wallrock compared to AFC. However, when assessed as a percentage of the resident magma system, this assimilated mass represents only ~ 29 wt.% of the final magma body (melt + crystals + fluid phase)—in contrast to 41 wt.% of the final magma body in the AFC case (Fig. 7b); thus, although the mass assimilated is larger, the addition of recharge magma "dilutes" the crustal signature. Like in the R_2FC case (compared to FC), the size of the magma body system (melt + cumulate + fluid phase, 352 m.u.) is substantially greater than in AFC (Fig. 3).

Discussion

It is instructive to compare outcomes of the cases described above (FC, R_2FC, AFC, S_2FC, R_2AFC) to illustrate how fractional crystallization, recharge, and contamination (by assimilation of wallrock partial melts or by assimilation of stoped blocks) affect the evolution of the composite shallow crustal magma system. We have purposely kept the compositions of M, WR, and R magmas constant to focus upon process and sequence rather than subsystem compositional variations. These five cases reflect a very small fraction of possible RASFC scenarios, but they underscore some of the challenges petrologists face in trying to identify crustal processes that dictate magma compositions.

Comparison of Thermal and Mass Characteristics

The final modeled wallrock temperature is related to the overall size of the magma body, the mass of cumulates formed, and the mass and thermodynamic state of the recharge magma/anatectic melt/stoped blocks added to the magma system. AFC and R_2AFC provide a contrast that illustrates the impact of magma recharge; the final wallrock temperature of R_2AFC (965 °C) is higher than that of AFC (852 °C), reflecting the addition of recharge magma with its attendant enthalpy (Fig. 6). All other parameters of these simulations are the same, including the initial wallrock temperature of 700 °C. The added enthalpy from hotter recharge magma into resident magma yields a larger increase in wallrock temperature during resident magma cooling and crystallization. Not only is there more resident magma to cool (i.e., more sensible heat), but also the mass of crystals formed in R_2AFC is

also greater, adding more latent heat of crystallization. The higher final wallrock temperature also means that wallrock melts to a greater extent for R_2AFC than AFC (56 wt.% versus 42 wt.%, respectively). More anatectic melt is transferred into the magma body per decrement of magma cooling (Fig. 7a), and thus, the cumulative amount of wallrock partial melt transferred is larger in R_2AFC. However, while the total mass of anatectic melt added to resident melt is larger in R_2AFC than AFC (~ 102 versus 71 m.u.; Fig. 7a), the percentage of the magma system mass that comes from anatectic melt is smaller (29 wt.% in R_2AFC versus 41 wt.% in AFC; Fig. 7b) due to the added recharge magma mass that makes the R_2AFC total magma system mass larger (~ 352 versus 171 m.u. for R_2AFC versus AFC, respectively, Online Resource 2). These collective differences, although perfectly clear in hindsight, are neither trivial nor easily predicted. They also bring into focus the difficulty of defining "rates" or amounts of assimilation. Furthermore, the enhancement of assimilation in systems with significant recharge might not be obvious geochemically due to the effects of recharge in diluting the geochemical signature of assimilated partial melt. Even in this simple comparison, one notes the complex feedbacks that can take place. The magnitude of these non-linear compositional effects varies depending on most of the sensible parameters of a given simulation. Although it is difficult to make broad brush statements, appreciation of these complex feedbacks clearly emerges once the MCS RAFC models are computed.

The final wallrock temperatures for FC, R_2FC and S_2FC are 329 °C, 656 °C, and 296 °C (Fig. 2), respectively. The lowest temperature of the stoping case is due to addition of cold blocks of wallrock. In addition, minerals in the blocks such as quartz and alkali feldspar are not stable after the blocks equilibrate with M melt. The energetic cost of resorbing these is debited to the magma, and thus magma has less enthalpy available to transfer to wallrock. The higher final WR temperature of R_2FC of 656 °C (compared to FC and S_2FC) is a function of added enthalpy due to recharge and underscores the energy impact and thermal priming potential that recharge can have: with two recharge events of modest recharge to initial magma mass ratio (0.75), the wallrock temperature increases from its initial (100 °C) to a temperature that reflects a relatively high geothermal gradient akin to the assimilation cases presented here. While different parameters will yield different outcomes, these examples highlight the potential for thermal priming via recharge.

The total mass of the magma system (which does not include the residual wallrock) is an obvious outcome of MCS, and one that is simple to contrast. FC, a "closed-system" process, yields the smallest magma body size, where the magma body includes resident magma melt + cumulates + fluid phase. The AFC and S_2FC cases are ~ 1.5 to 1.7 × bigger than the FC magma body, R_2FC is ~ 2.5 × bigger, and R_2AFC is the biggest at ~ 3.5 × (Online Resource 2; these comparisons relate masses upon completion of the simulations). These differences are obviously related to addition of recharge magma, anatectic melt and/or stoped crustal blocks and have implications for the sizes of

potential eruptions, the growth of the crust (i.e., mass of magma added to the crust), its state of stress, and local geotherms.

Another difference, not necessarily obvious, is the percent melt versus crystals among these different magma systems. AFC and R_2AFC suppress crystallization, compared to the other cases. In the AFC and R_2AFC cases, the cumulate reservoir composes about 38–43 wt.% of the resident magma system, whereas it is ~ 76 wt.% of the magma body mass in the FC and R_2FC cases; S_2FC yields approximately 67 wt.% crystals (Fig. 3d). Suppression of crystallization is caused by addition of anatectic melt, which changes the temperature–composition relationships such that the mass of crystals that form per decrement of cooling of M melt is lower when assimilation is ongoing (e.g., the slope of the magma temperature versus percent cumulative crystals is lower for AFC and for the assimilation-influenced parts of the R_2AFC compared to FC and R_2FC, Fig. 3d). Thus, in the two cases that invoke assimilation, the magma system is dominated by melt: 57 wt.% for AFC and 62 wt.% for R_2FC (Fig. 3b). The higher equilibration temperature for R_2AFC plays a role in the high proportion of melt, but even if the slope of the R_2AFC magma temperature versus percent cumulative crystals trend (Fig. 3d) is extrapolated to a higher final magma temperature, the percent crystals is still lower than the R_2FC and FC cases. Note that although the proportion of crystals in R_2AFC is smaller than in FC and S_2FC (Fig. 3d), the total mass of crystals is larger (Fig. 3c), as expected from the larger total system mass. This outcome leads to the prediction that basaltic systems recharged with magmas similar to the initial parent magma will build large cumulate piles whereas basaltic systems that experience contamination by average upper crust may be melt dominated systems.

Explicit tracking of instantaneous and cumulative masses of minerals crystallized and anatectic melt assimilated (versions of the DePaolo (1981) "*r*", which was defined in this paper as mass assimilation rate/mass fractional crystallization rate) provides a platform by which to examine the ratio of mass of anatectic melt assimilated to the mass of cumulates formed during AFC. Here, instantaneous refers to the ratio of the mass of anatectic melt assimilated divided by the mass of crystals formed in a single (circa 5 °C) AFC magma temperature decrement (i.e., crystallization followed by assimilation); in the case when recharge occurs (R_2AFC), the crystal mass includes crystals formed upon recharge added to those formed in a fractional crystallization "event." Cumulative refers to the total mass of anatectic melt divided by the total mass of crystals from the first step in the simulation to the present temperature step. For AFC, instantaneous and cumulative "*r*" values vary from 0.71 to 2.6 and 0.13 to 0.99, and for R_2AFC from 0.16 to 2.0 and 0.13 to 0.83, respectively (values reflect start of assimilation to end of the simulation, Fig. 8). For the first part of the AFC instantaneous and cumulative trends (from M melt temperate of ~ 1055–930 °C), the productivity of melt in wallrock systematically increases as magma temperature goes down. The marked change (decrease) in instantaneous "*r*" between ~ 930 and 922 °C reflects decreased anatectic melt productivity because alkali feldspar is no longer part of the wallrock assemblage; this change is

reflected in the change in slope of the cumulative plot as well (Fig. 8). The subsequent increase in instantaneous "*r*" is due to a decrease in the mass of crystals produced with each AFC "event".

For the R_2AFC case, instantaneous and cumulate "*r*" are the same as AFC until the first recharge event. Upon recharge (event 1, R_2AFC, Fig. 8a), instantaneous "*r*" increases systematically (offset to a higher temperature due to the effects of recharge), because the mass of anatectic melt transferred from wallrock after the recharge events is higher than before; this leads to an increase in instantaneous "*r*". The decrease in R_2AFC instantaneous "*r*" at temperatures between ~ 1020 and 998 °C (before recharge event 2) occurs because alkali feldspar in the wallrock is fully reacted, and anatectic melt productivity decreases as a result. A consequence of the second recharge event (that brings the magma temperature up to ~ 1026 °C) is a short-lived pulse of crystallization that yields a decrease in both instantaneous and cumulative "*r*" (Fig. 8). Following this, the somewhat complex trend seen in the instantaneous "*r*" is the result of changes in crystallization as the magma system responds to being heated by recharge as well as the changing restitic mineral composition of wallrock and the associated consequences on wallrock melt production.

Three outcomes of the analysis above are that (1) crystallization and assimilation "rates" are difficult if not impossible to predict in the absence of thermodynamic treatment, and thus, (2) quantitative thermodynamic treatment of RAFC processes is absolutely essential to characterize these rates. Furthermore, (3) these rates are, therefore, neither predictable nor constant, and models that use constant "*r*" values as defined, for example, by DePaolo (1981) do not reflect the phase equilibria or energetic consequences of these processes. Given the availability of computational tools that provide thermodynamic estimations of magma systems, we suggest that tools that lack phase equilibria treatment of igneous systems may, at best, provide only rough estimates of natural processes and, therefore, should be used with considerable caution. In addition, one should be wary of conventional arguments and inferences often applied when analyzing petrological and geochemical data. Many of these notions are based on closed system behavior and/or bulk assimilation without inclusion of phase equilibria.

Geochemical and Petrological Indicators of Open-System Processes

The major oxide signatures of open-system magmatic processes manifest in ways that may not be obvious or intuitive. Among the best indicators of open-system processes are radiogenic and stable isotopes, assuming that there is isotopic contrast between resident magma, crust, and recharge magma. Why then toil to identify or quantify fingerprints of RASFC using major element data? The first reason is practical; typically, many more samples are analyzed for major elements than for isotopes and some trace elements. Second, careful reconstruction of major element characteristics as well as the crystallizing mineral assemblage is required for accurate calculation of trace element and

isotopic signatures of an open-system magma via the use of mineral/melt and mineral/fluid distribution coefficients. Thus, to document trace element and isotopic open system signatures, one must know the open-system history of melt, minerals, and fluid. The third reason is that a higher number of constraints (major oxides, trace elements, isotopes) leads to better models, and better models can lead to more refined interpretations. For example, determining whether a magma storage system is more likely located in the shallow versus deep crust has implications for volcanic eruption monitoring and hazard mitigation. All such models should naturally always be assessed in relation to MCS-independent evidence such as geophysical constraints. Fourth, as has been shown in numerous studies, in some cases isotopic contrast between magma and wallrock, for example, is lacking (e.g., Stern and Johnson 2010), and thus pursuit of open-system major element and phase equilibria models is an absolute necessity.

Below, we highlight major element and phase equilibria comparisons that illustrate the complexity of identifying open-system processes and that emphasize the value of thermodynamic modeling.

Identifying the Fingerprint of Magma Mixing from Melt and Mineral Data

Classic linear trajectories often ascribed to binary mixing are not present in many of the R_2FC major element plots (e.g., SiO_2 versus MgO, Na_2O, TiO_2; Fig. 4). This is because homogenization is followed by crystal removal through fractional crystallization. The inverse is also true; there are segments of some of the FC oxide arrays that are approximately linear (e.g., K_2O, P_2O_5, H_2O, Al_2O_3 at SiO_2 > ~55 wt.%), and thus may resemble mixing trends. Thus, the assumption that mixing can be diagnosed by linear trends is misleading.

The similarity of many oxide trends for FC and R_2FC (Fig. 4) underscores the difficulty of diagnosing process using such data. But some oxides can show distinctive behavior with recharge. In the simulations highlighted here, MgO is the most telling. Its concentration changes beyond analytical uncertainty when recharge with a more primitive magma occurs, but the difference between FC and R_2FC is subtle and might be difficult to detect in a suite of samples that lack stratigraphic control.

As recognized in numerous studies, crystal cargo (e.g., Davidson et al. 2007; Streck 2008, and references therein; Edwards et al. 2019, Ubide et al. 2019; Ubide and Kramer 2018; Streck et al. 2008; Ginibre et al. 2007; Davidson et al. 1997) can provide a rich inventory of mixing histories. Are MCS results applicable to such data? The answer is yes, with careful consideration of the design features of MCS. The current version of MCS immediately fractionates all crystals, and thus zoned crystals are technically not produced and no resorption of cumulates is permitted. What is produced is a sequential record of crystallization. The crystals that are fractionated into a separate cumulate reservoir during progressive RFC "events" can be reimagined as growing, zoned crystals that remain in the M melt and interact thermally but not chemically with host magma; the mass and energy

balance for such zoned crystals is the same as it is for crystals fractionated to the cumulate reservoir. By using the sequential record and carefully applying it to crystal cargo data (subject to the limitation in the current version of MCS that crystals do not chemically interact with M melt), one can utilize MCS results to better understand possible crystal behavior that results from RASFC.

Envisioning crystals as growing in this way, the R_2FC modeling results indicate that in some cases, the record of recharge may be selective. In R_2FC, the complete record of mixing is not preserved in plagioclase, which is not stable upon mixing, but returns to the stable assemblage within ~ 25 °C of cooling after the first recharge event and ~ 5 °C of cooling after the second. Its compositional change is small after the first event (An_{81} to An_{82}) but larger and detectable after the second (An_{71} to An_{77}). In stark contrast to plagioclase behavior, olivine crystallizes both before and after mixing, thus recording a complete phase equilibria record of the effects of mixing. The mineral changes composition abruptly from Fo_{70} to Fo_{78} after the first recharge/mixing event, and from Fo_{55} to Fo_{68} after the second event. These changes are easily detected by electron microprobe analysis, provided the zoning is preserved.

Crystals produced during mixing may also preserve a record of temperature changes. For R_2FC, the temperature of the magma increases 40–50 degrees after each mixing event. That record may be preserved in mineral geothermometry. In R_2FC, olivine and clinopyroxene would be the best indicators of the temperature change, as they preserve the most complete record of mixing. In contrast, plagioclase would not likely record heating associated with the first recharge event for the reasons discussed in the previous paragraph. The takeaway lesson from this single example is that to fully document temperature excursions associated with recharge that are recorded in minerals, one needs a complete picture of the phase equilibria changes that occur in response to the mixing event. Even with such data, documenting temperature changes may be challenging given the equilibrium requirements and uncertainties of many geothermometers (e.g., Putirka 2017).

The presence or absence of distinctive recharge signatures is a function of the magma mixing scenario. In the cases highlighted here, the same parent magma is mixed into its evolving counterpart. Different scenarios will lead to different mixing fingerprints. For example, the mass of the recharge event compared to the resident magma/melt mass will influence the extent to which pre- and post-recharge magmas change composition, and a substantial compositional contrast between resident melt and recharge magma may yield recharge signatures that are more obvious than those presented here. Myriad forward modeling case studies can be done in MCS to examine the temperature, composition, and mass landscape of mixing and crystallization processes.

Identifying the Fingerprint of Crustal Assimilation from Melt and Mineral Data

Similar to the FC versus R_2FC comparison, some major oxides do not show evidence of crustal assimilation. For example, AFC and R_2AFC are generally similar to FC and R_2FC in SiO_2 versus

MgO (with the exception of the notable change immediately after the recharge events for R_2AFC and R_2FC) and CaO (Fig. 4). This is an interesting result given the anatectic melt and recharge magma have very different concentrations of these oxides, and yet, the SiO_2 versus CaO and MgO trends are indistinguishable for these four cases at > 55 wt.% SiO_2.

In contrast, three major elements that show quite distinct differences are K_2O, Na_2O, and Al_2O_3 (Fig. 4). Once assimilation begins, Al_2O_3 is more concentrated in AFC and R_2AFC than in their non-assimilation equivalents (at the same SiO_2). Because these cases contrast with respect to not just the bulk composition of the added anatectic melt, but also in the mass and identity of cumulus phases, there could be a number of explanations for these differences. The total final percentage of cumulus plagioclase in FC and AFC is similar (~ 39 wt.%), whereas for R_2AFC, it is smaller (~ 26 wt.%) (Fig. 5c). Thus, for FC and AFC, about the same final proportional amount of plagioclase was removed as a fractionating phase, but that final tally obscures differences as the systems evolve. Reference to Fig. 5c shows that plagioclase makes up a smaller proportion of the cumulate assemblage in AFC, compared to FC, for most of the simulation. The reason the final proportions are similar is because the end temperature of AFC (~ 856 °C) is lower than that for FC (~ 899 °C), which provides a slightly longer crystallization temperature interval for plagioclase in the AFC case. For most of the AFC simulation, for each cooling step, less plagioclase forms, and thus the resident melt is not debited in Al_2O_3 as extensively as in the FC case (Fig. 4b). In the case of R_2AFC, Al_2O_3 is slightly higher at the same wt.% SiO_2 than in the AFC case and reflects the lower cumulate plagioclase proportion, compared to AFC (Fig. 5c). Thus, less Al_2O_3 is removed from resident melt. R_2AFC and AFC have distinctly lower Na_2O at the same SiO_2 (once assimilation begins), whereas K_2O is distinctly higher than FC and R_2FC (Fig. 4g, h). The bulk composition of wallrock and the way it melts are responsible for these differences. Alkali feldspar melts disproportionately into anatectic melt, enriching the melt in K_2O. Plagioclase (~ $An_{37–35}$), on the other hand, disproportionately increases in abundance in wallrock restite, and thus, anatectic melt addition dilutes Na_2O in resident magma melt. All these changes are recorded in the respective output files in the Online Resource 6.

Resident melt H_2O is less concentrated in AFC and R_2AFC compared to FC and R_2FC (Fig. 4j) due to an assumption imposed on the current version of MCS. As discussed in the Section entitled "Case 3: Assimilation–Fractional Crystallization (AFC)", while wallrock is fluid-saturated upon initiation of melting, the fluid phase is not incorporated into magma melt although H_2O dissolved in anatectic melt is. Once assimilation begins, dilution due to anatectic melt addition is evident, and lower rates of crystallization (i.e., mass of crystals fractionated per decrement of cooling in resident magma) of anhydrous minerals in the AFC case lessens the amount of H_2O enrichment. R_2AFC parallels the AFC trend until the first recharge event, which dilutes H_2O. The second causes additional dilution. The combination of recharge and lower rates of crystallization yields the lowest magma melt H_2O contents of all the cases by the termination of the simulation. The remaining oxides also show

differences, but these are less pronounced and are due to differences in anatectic melt versus magma melt compositions and the associated phase equilibria differences between the FC and AFC cases.

Based on the analysis above, for the AFC and R_2AFC cases presented here in which a depleted basalt is being contaminated by anatectic melt from average upper continental crust, the only major element and phase equilibria indicators that are likely to be diagnostic are the resident melt K_2O, which is enriched by ~ 5 × by the end of the AFC versus FC simulation (Fig. 4h). An expectation that crustal assimilation would lead to more profound and obvious changes in other oxides might yield a misinterpretation of these data that attributes the geochemical signals to mantle heterogeneity. Likewise, depletion of Na_2O might be easily misinterpreted as representative of mantle heterogeneity and/or alteration. While the AFC/R_2AFC Al_2O_3 versus SiO_2 trends are distinct from those of FC, Al_2O_3 may be difficult to interpret as its concentration is partly a function of the amount of plagioclase crystallization, which may vary according to crystallization conditions. While we recognize that these results are case specific, they underscore the importance of open-system models that evaluate phase equilibria.

Mineral fingerprints of assimilation are potentially preserved in the cumulate assemblage. The most obvious is the presence of orthopyroxene, which is not stable in FC and is in much smaller proportion in R_2FC (~ 1 wt.%) compared to > 10 wt.% for AFC and R_2AFC (Fig. 5f). Orthopyroxene is stabilized by SiO_2 added by anatectic melt; on the other hand, fractionation of orthopyroxene enriches M melt in SiO_2 less than crystallization of olivine so the effect of adding SiO_2 into the system by assimilation is counteracted (Fig. 4). Other wt.% differences for the cumulate assemblages are evident. For example, olivine and clinopyroxene do not crystallize for the full AFC simulation whereas they do in FC.

Similar to predictions about the effects of magma recharge and mixing, the case studies involving assimilation bring into focus the difficulty of postulating a priori the patterns expected on element and oxide variation diagrams and in mineral compositions and identities. Major element and mineralogical responses to these processes may not be easily predicted or distinguished. The overarching conclusion of the recharge and assimilation case studies is that using closed system reasoning may produce misleading and spurious conclusions, because the effects of open-system processes are non-linear and, in many cases, non-intuitive.

Distinguishing the Mode of Crustal Contamination: Crustal Assimilation versus Stoping

Here, we compare and contrast AFC and S_2FC to illustrate a possible range of effects from different mechanisms of crustal contamination. As anticipated, evidence of bulk assimilation of stoped blocks compared to assimilation of anatectic melt is preserved in some oxide trends, but not in others.

In the S_2FC scenario, SiO_2 versus MgO and CaO are quite similar to AFC, and TiO_2, Fe_2O_3, and P_2O_5 show only subtle differences (Fig. 4). In contrast, Al_2O_3, FeO, K_2O, Na_2O, and H_2O are markedly different for AFC versus S_2FC. For the first stoping event, Al_2O_3 versus SiO_2 has a slope that is rather similar to FC and R_2FC trends, and thus is much lower in concentration (at the same SiO_2) compared to AFC. While the Al_2O_3 content of the stoped block is slightly higher than M melt, addition of the stoped block (with its Al_2O_3) is apparently offset by a "pulse" of plagioclase crystallization (described in the next paragraph) that removes Al_2O_3. While intuition may dictate that adding an Al-rich stoped block would lead to increased Al_2O_3 in M melt, this will not always be the case and this example again illustrates how simplistic reasoning can be misleading (e.g., polyphase mixing is not identical to melt–melt mixing). Likewise, Al_2O_3 remains at lower concentrations compared to AFC during and after the second stoping event for the same reason. Spinel also experiences a pulse of crystallization with both stoping events, and likely contributes to the lower Al_2O_3 in the S_2FC case. S_2FC Na_2O is higher than AFC (Fig. 4g); by the first stoping event, Na_2O in the stoped block is much higher than in the equivalent anatectic melt (i.e., at approximately, the same wallrock temperature), and thus Na_2O in the S_2FC case is higher than in the AFC case. K_2O is the opposite (Fig. 4h). S_2FC K_2O is not as enriched as in the AFC case, because the stoped block K_2O concentration is lower than that of anatectic melts. These differences are both a direct result of the difference in style of contamination. Through assimilation by stoping, bulk wallrock contaminates M melt, whereas the process of partial melting during AFC enriches K_2O content and depletes Na_2O in anatectic melt. H_2O is more enriched at a given SiO_2 in S_2FC than in AFC, because, in the current version of MCS, all of the fluid phase is transferred into resident melt via stoping, as opposed to remaining in wallrock restite in the AFC case.

Assimilation by stoping also has an effect on the cumulate assemblage. Upon homogenization of the first stoped block, all of the quartz and alkali feldspar react away. As noted above, a "burst" (i.e., large mass) of plagioclase crystallizes (Fig. 5c; 7.5 × more than had been crystallizing in prior magma temperature decrements) in response to assimilation of the stoped block. Spinel also experiences a crystallization burst (Fig. 5d; increase by 7 ×), but the total mass is much smaller than plagioclase. Similar to stoping event 1, during homogenization of stoped block 2, quartz completely reacts, and, plagioclase and spinel crystallization bursts occur, and these are proportionally much larger than after stoping event 1 (Fig. 5; e.g., for plagioclase, ~ 30 × more than had been crystallizing in prior magma temperature decrements). While plagioclase continuously crystallizes in both AFC and S_2FC, the mass, thermal and compositional records are quite different. In AFC, each set of fractional crystallization-assimilation "events" yields about the same mass of plagioclase, and its composition varies smoothly from An83 when assimilation begins to An_{54} at the simulation's termination. The temperature record is also smoothly varying with decreases of ~ 15 °C per fractional crystallization-assimilation "event". For stoping events 1 and 2, there is a dramatic increase in the mass rate of

plagioclase crystallization and an abrupt change in plagioclase Na content (from An_{75} to An_{65} for event 1, and from An_{51} to An_{38} for event 2), and the melt temperature decreases are ~ 47 °C and 45 °C, respectively. Both of these changes would be detectable by modern analytical methods and geothermometers. By the end of the simulation, plagioclase in S_2FC is distinctly more albitic than that in AFC (An_{37} versus An_{54}), consistent with the addition of Na_2O from stoped blocks compared to the "dilution" effect seen in AFC due to partial melting of wallrock. The difference in plagioclase composition highlights the difference in bulk addition of a stoped block versus addition of partial melt from wallrock. Partial melting favors reaction of alkali feldspar over plagioclase, and thus the resulting anatectic melts substantially enriches resident melt in K and depletes it in Na. These elemental differences influence the M melt phase equilibria response.

Quantifying Mantle versus Crustal Contributions to Magma Systems

A key goal in petrology and geochemistry—to distinguish and quantify how mantle versus crustal contributions to a magma system change in space and time—informs models of crustal growth and evolution, models of mantle evolution, and mass and thermal fluxes between these reservoirs. The literature abounds with studies of magmatic systems in which geochemical and petrologic signatures are quantitatively or qualitatively attributed to mantle versus crust (e.g., Hildreth and Moorbath 1988; Asmerom et al. 1991; Arndt et al. 1993; Wooden et al. 1993; Baker et al. 2000). Modeling results presented here illustrate the complexity associated with this enterprise and some potential pitfalls. The FC case assumes that mantle-derived magma intrudes the crust and undergoes fractional crystallization without involvement of any crust. Thus, the entire compositional signal derives from the mantle mediated by low-pressure crystal fractionation. Magmas that have undergone only fractional crystallization without interaction with crust and/or without magma mixing are probably uncommon given the realities of moving low-viscosity materials through large sections of crust of contrasting composition as well as the episodic nature of magma intrusion. The case of FC only is, therefore, admittedly a simplification but serves as a point of comparison. Discussion of how the mass of mantle versus crust is portrayed, as discussed in the Section "Comparison of thermal and mass characteristics" underscores the challenges with quantifying crust versus mantle.

Based on many thousands of MCS models, we have collectively run over the past several years, we suggest a top-down approach to distinguishing crust versus mantle contributions. That is, we recommend characterizing and quantifying possible open system crustal processes first. Once plausible and potential RASFC scenarios are fully explored (i.e., running many MCS models), remaining discrepancies between model results and data from a natural system might then be postulated to be caused by mantle heterogeneity of the M subsystem magma.

Magma Chamber Simulator: Ongoing Developments

The MCS has undergone continuous development and improvement since its first incarnation and we continue to expand its functionality. Here we review four major extensions presently under development.

A critical enhancement of MCS is to free it from its dependence on Excel, which is a temperamental platform on which to build and sustain development. A high priority for MCS is to port the code to a new platform with an accessible web user interface. The second enhancement addresses the limitation that cumulate crystals cannot react with M melt. It is well established in the rock record that crystal (cumulate)–melt interaction occurs. As one example, the concept of crystal resorption has been part of the petrological literature for a long time (e.g., Fries 1939; Wiebe 1968; Couch et al. 2001; Ginibre et al. 2007; Erdmann et al. 2012); orthopyroxene rims on olivine-cored crystals is perhaps the type example (e.g., Ambler and Ashley 1977). MCS will be modified to allow some fraction of earlier formed cumulates to react with M melt. A third MCS future development, as noted, is to allow transfer of some proportion of the fluid phase in wallrock to transfer into M melt. Finally, planning is underway to implement a Monte Carlo version of the MCS. To run a single R_2AFC simulation like the one illustrated here, circa 80 parameters should be specified in the MES input file (including all the oxides for magma, wallrock, and recharge magmas). In attempting to model a natural system, one recognizes that there are inherent uncertainties in these parameters. Therefore, the MCS algorithm will be extended by adoption of a Monte Carlo approach by allowing each input parameter to be specified as a possible range of values (e.g., SiO_2 of the wallrock lies between 67 and 69 wt.% etc.). Once ranges for all input parameters have been defined, the algorithm will select randomly or by Bayesian methods a particular set of initial conditions. In this manner, thousands or even tens of thousands of MCS models can be run, each with a unique set of input parameters and associated output. Once archived in a searchable database, the user can then ask questions such as: Of the thousands of simulations run, which ones compare best to the data from the particular natural system under study? Using this Monte Carlo approach, solutions can be filtered to find the best fit to observables using some objective criterion such as the residuals of the squared differences between the model and the observations.

Conclusions

Analysis of attributes of igneous systems suggests that open system behavior is dominated by crystal fractionation, magma mixing, and the interaction of magmas with their host environments via partial melting and stoping of wallrock. An important task for the petrologist/geochemist is to unravel the most important RASFC processes by quantification and temporal ordering. Establishing a

magmatic 'arrow of time' is intrinsically a complex task due to the vast range of temporal and spatial scales involved—from microns to kilometers and from hours to several million years. Deciphering such records demands a variety of approaches.

As precision and spatial resolution of analyses of magmatic products have improved, so has the petrologist's ability to quantify the magmatic processes that generate compositional diversity. Forty years of progress have seen improvements in modeling, from those that focused exclusively on mass balance, to mass and enthalpy balance, to those that are underpinned by a thermodynamic database. The Magma Chamber Simulator is a mass- and energy-balanced, thermodynamic tool that addresses open-system magmatic processes that govern the evolution of a multicomponent–multiphase composite system of wallrock, resident magma, and recharge/stoping reservoirs. MCS-PhaseEQ models the major element and phase equilibria consequences of RASFC, and MCS-Traces, the subject of a companion paper, models trace elements and isotopes. MCS-PhaseEQ relies on rhyolite- and pMELTS as its thermodynamic engine and Visual Basic as its executive brain. MCS provides significant insight into crustal magma processes and the origin of compositional diversity via modeling how variations in specific input (e.g., pressure, parental magma composition, wallrock initial temperature, number and mass of recharge events) contribute to magma diversity and eruptability. Systematic modeling of this sort affords the development of a framework for systematizing potentially distinctive characteristics of RASFC processes. MCS forward modeling also abounds with potential for describing the evolution of particular volcanic and plutonic rock suites, thus providing a quantitative framework for interpreting the remarkable and abundant compositional and isotopic data sets that are now routinely generated for igneous rocks. The five case studies we discuss (FC, R_2FC, AFC, S_2FC, and R_2AFC) illustrate the rich data set that MCS produces and elucidate both the challenges of identifying open system processes from major element and phase equilibria data and the utility of using open-system thermodynamic models such as MCS to document open magma systems.

Online Resources

Online Resource 1: Characteristics of Recharge or Stoping Events

Online Resource 2: Mass and Temperature Outcomes for Five MCS cases

Online Resource 3: Mineral Mass and Composition Data and Melt Composition Data

Online Resource 4: Wallrock Characteristics

Online Resource 5: Characteristics of Recharge or Stoping Events

Online Resource 6: MCS output for FC, R_2FC AFC, S_2FC, and R_2AFC

Online Resource 7: MCS input for FC, R_2FC AFC, S_2FC, and R_2AFC

Online Resource 8: MCS Visualizer animations for FC, R_2FC AFC, S_2FC, and R_2AFC

Online Resource 9: Results of WR fluid transfer modeling with rhyolite-MELTS

Acknowledgements

We are indebted to numerous MCS users and workshop attendees who have contributed to improving MCS. We also thank CWU students Jennifer McLeod, Alec Melone, Rachel Sanchez, and Rebekah Krohn for their work on improving MCS. We also send a hearty thank you to Dr. Mark Ghiorso, whose cooperation in developing MCS, was critical. We thank an anonymous reviewer and Paul Asimow for insightful reviews and Othmar Müntener for his expert editorial handling. This work was funded by NSF grants to WA Bohrson and FJ Spera and by the Academy of Finland grants 295129 and 306962 to JS Heinonen and E. Suikkanen.

References

1. Albarède F (1995) Introduction to geochemical modeling. Cambridge University Press, Cambridge
2. Ambler EP, Ashley PM (1977) Vermicular orthopyroxene-magnetite symplectites from the Wateranga layered mafic intrusion, Queensland, Australia. Lithos 10:163–172. https://doi.org/10.1016/0024-4937(77)90044-5
3. Arndt NT, Czamanske GK, Wooden JL, Fedorenko VA (1993) Mantle and crustal contributions to continental flood volcanism. Tectonophysics 223:39–52. https://doi.org/10.1016/0040-1951(93)90156-e
4. Asimow PD, Ghiorso MS (1998) Algorithmic modifications extending MELTS to calculate subsolidus phase relations. Am Miner 83:1127–1131
5. Asmerom Y, Patchett PJ, Damon PE (1991) Crust-mantle interaction in continental arcs: inferences from the Mesozoic arc in the southwestern United States. Contrib Mineral Petrol 107:124–134. https://doi.org/10.1007/BF00311190
6. Baker JA, Macpherson CG, Menzies MA, Thirlwall MF, AL-Kadasi M, Mattey DP (2000) Resolving crustal and mantle contributions to continental flood volcanism, Yemen; constraints from mineral oxygen isotope data. J Petrol 41:1805–1820. https://doi.org/10.1093/petrology/41.12.1805
7. Becerril L, Galindo I, Gudmundsson A, Morales JM (2013) Depth of origin of magma in eruptions. Sci Rep 3:2762. https://doi.org/10.1038/srep02762
8. Bohrson WA, Spera FJ, Ghiorso MS, Brown GA, Creamer JB, Mayfield A (2014) Thermodynamic model for energy-constrained open-system evolution of crustal magma bodies undergoing simultaneous recharge, assimilation and crystallization: the magma chamber simulator. J Petrol 55:1685–1717. https://doi.org/10.1093/petrology/egu036
9. Borisova AY, Bohrson WA, Grégoire M (2017) Origin of primitive ocean island basalts by crustal gabbro assimilation and multiple recharge of plume-derived melts. Geochem Geophys Geosyst 18:2701–2716. https://doi.org/10.1002/2017GC006986
10. Bowen NL (1928) The evolution of igneous rocks. Dover Publications, New York, p 334
11. Coogan LA, Saunders AD, Wilson RN (2014) Aluminum-in-olivine thermometry of primitive basalts: evidence of an anomalously hot mantle source for large igneous provinces. Chem Geol 368:1–10. https://doi.org/10.1016/j.chemgeo.2014.01.004
12. Costa F, Dohmen R, Chakraborty S (2008) Time scales of magmatic processes from modeling the zoning patterns of crystals. In: Putirka KD, Tepley FJ III (eds) Minerals, inclusions and volcanic processes, vol 69. Mineralogical Society of America, Chantilly, pp 545–594. https://doi.org/10.2138/rmg.2008.69.14

13. Couch S, Sparks RSJ, Carroll MR (2001) Mineral disequilibrium in lavas explained by convective self-mixing in open magma chambers. Nature 411:1037–1039. https://doi.org/10.1038/35082540

14. Cox KG, Hawkesworth CJ (1984) Relative contribution of crust and mantle to flood basalt magmatism, Mahabaleshwar area, Deccan Traps. Philos Trans Royal Soc London Ser A, Math Phys Sci 310:627–641. https://doi.org/10.1098/rsta.1984.0011

15. Davidson JP, Tepley FJ (1997) Recharge in volcanic systems: evidence from isotope profiles of phenocrysts. Science 80(275):826–829. https://doi.org/10.1126/science.275.5301.826

16. Davidson JP, Morgan DJ, Charlier BLA, Harlou R, Hora JM (2007) Microsampling and isotopic analysis of igneous rocks: implications for the study of magmatic systems. Ann Rev Earth Planet Sci 35:273–311

17. DePaolo DJ (1981) Trace element and isotopic effects of combined wallrock assimilation and fractional crystallization. Earth Planet Sci Lett 53:189–202. https://doi.org/10.1016/0012-821x(81)90153-9

18. Edwards MA, Jackson MG, Kylander-Clark ARC, Harvey J, Hagen-Peter GA, Seward GGE, Till CB, Adams JV, Cottle JM, Hacker BR, Spera FJ (2019) Extreme enriched and heterogenous $^{87}Sr/^{86}Sr$ ratios recorded in magmatic plagioclase from the Samoan hotspot. Earth Planet Sci Lett 511:190–201. https://doi.org/10.1016/j.epsl.2019.01.040

19. Erdmann S, Scaillet B, Kellett DA (2012) Textures of peritectic crystals as guides to reactive minerals in magmatic systems: new insights from melting experiments. J Petrol 53:2231–2258. https://doi.org/10.1093/petrology/egs048

20. Fries C (1939) Resorbed feldspar in a basalt flow. Am Mineral 24(12):782–790

21. Ghiorso MS, Sack RO (1995) Chemical mass transfer in magmatic processes IV. A revised and internally consistent thermodynamic model for the interpolation and extrapolation of liquid-solid equilibria in magmatic systems at elevated temperatures and pressures. Contrib Mineral Petrol 119:197–212. https://doi.org/10.1007/bf00307281

22. Ghiorso MS, Gualda GAR (2015) An H2O–CO2 mixed fluid saturation model compatible with rhyolite-MELTS. Contrib Mineral Petrol 169:53. https://doi.org/10.1007/s00410-015-1141-8

23. Ghiorso MS, Hirschmann MM, Reiners PW, Kress VC III (2002) The pMELTS: a revision of MELTS for improved calculation of phase relations and major element partitioning related to partial melting of the mantle to 3 GPa. Geochem Geophys Geosyst 3:1–35. https://doi.org/10.1029/2001GC000217

24. Ginibre C, Wörner G, Kronz A (2007) Crystal zoning as an archive for magma evolution. Elements 3:261–266. https://doi.org/10.2113/gselements.3.4.261

25. Grove TL, Kinzler RJ, Bryan WB (1992) Fractionation of mid-ocean ridge basalt (MORB). In: Morgan JP, Blackman DK, Sinton JM (eds) Mantle flow and melt generation at mid-ocean ridges, geophysical monograph series. Geophysical monograph series, vol 71. American Geophysical Union, Washington, pp 281–310. https://doi.org/10.1029/GM071p0281

26. Gualda GAR, Ghiorso MS, Lemons RV, Carley TL (2012) Rhyolite-MELTS: a modified calibration of MELTS optimized for Silica-rich, fluid-bearing magmatic systems. J Petrol 53:875–890. https://doi.org/10.1093/petrology/egr080

27. Heinonen JS, Luttinen AV, Spera FJ, Bohrson WA (2019) Deep open storage and shallow closed transport system for a continental flood basalt sequence revealed with Magma Chamber Simulator. Contrib Mineral Petrol 174(11):87

28. Heinonen JS, Bohrson WA, Spera FJ, Brown GA, Scruggs M, Adams J (2020) Diagnosing open-system magmatic processes using the Magma Chamber Simulator (MCS): part II—trace elements and isotopes. Contrib Mineral Petrol. https://doi.org/10.1007/s00410-020-01718-9

29. Hildreth W, Moorbath S (1988) Crustal contributions to arc magmatism in the Andes of Central Chile. Contrib Mineral Petrol 98:455–489. https://doi.org/10.1007/BF00372365

30. Lesher CE, Spera FJ (2015) Thermodynamic and transport properties of silicate melts and magma. In: Sigurdsson H (ed) The encyclopedia of volcanoes, 2nd edn. Academic Press, Amsterdam, pp 113–141. https://doi.org/10.1016/b978-0-12-385938-9.00005-5

31. Luttinen AV, Furnes H (2000) Flood basalts of Vestfjella: Jurassic magmatism across an Archaean-Proterozoic lithospheric boundary in Dronning Maud Land, Antarctica. J Petrol 41:1271–1305. https://doi.org/10.1093/petrology/41.8.1271

32. Mangiacapra A, Moretti R, Rutherford M, Civetta L, Orsi G, Papale P (2008) The deep magmatic system of the Campi Flegrei caldera (Italy). Geophys Res Lett. https://doi.org/10.1029/2008GL035550

33. Moore NE, Grunder AL, Bohrson WA (2018) The three-stage petrochemical evolution of the Steens Basalt (southeast Oregon, USA) compared to large igneous provinces and layered mafic intrusions. Geosphere 14:2505–2532. https://doi.org/10.1130/GES01665.1

34. Neave DA, Putirka KD (2017) A new clinopyroxene-liquid barometer, and implications for magma storage pressures under Icelandic rift zones. Am Min 102:777–794. https://doi.org/10.2138/am-2017-5968

35. Oldenburg CM, Spera FJ, Yuen DA, Sewell G (1989) Dynamic mixing in magma bodies: theory, simulations, and implications. J Geophys Res 94:9215–9236. https://doi.org/10.1029/JB094iB07p09215

36. Powell R, Holland TJB (1988) An internally consistent dataset with uncertainties and correlations: 3. Applications to geobarometry, worked examples and a computer program. J Metamorph Petrol. https://doi.org/10.1111/j.1525-1314.1988.tb00415.x

37. Powell R, Holland TJB (1994) Optimal geothermometry and geobarometry. Am Mineral 79:120–133

38. Powell R, Holland TJB, Worley B (1998) Calculating phase diagrams involving solid solution via non-linear equations, with examples from THERMOCALC. J Metamorph Petrol. https://doi.org/10.1111/j.1525-1314.1998.00157.x

39. Putirka KD (2008) Excess temperatures at ocean islands: implications for mantle layering and convection. Geology (Boulder) 36:283–286. https://doi.org/10.1130/G24615A.1

40. Putirka K (2017) Geothermometry and geobarometry. In: White WM (ed) Encyclopedia of geochemistry: a comprehensive reference source on the chemistry of the Earth. Springer International Publishing, Cham, pp 1–19. https://doi.org/10.1007/978-3-319-39193-9_322-1

41. Rudnick RL, Gao S (2003) The composition of the continental crust. In: Rudnick RL (ed) The crust, treatise on geochemistry, vol 3. Elsevier-Pergamon, Oxford, pp 1–64. https://doi.org/10.1016/b0-08-043751-6/03016-4

42. Scruggs MA, Putirka KD (2018) Eruption triggering by partial crystallization of mafic enclaves at Chaos Crags, Lassen Volcanic Center, California. Am Min 103:1575–1590

43. Spera FJ, Bohrson WA (2001) Energy-constrained open-system magmatic processes I: general model and energy-constrained assimilation and fractional crystallization (EC-AFC) formulation. J Petrol 42:999–1018. https://doi.org/10.1093/petrology/42.5.999

44. Spera FJ, Schmidt JS, Bohrson WA, Brown GA (2016) Dynamics and thermodynamics of magma mixing: Insights from a simple exploratory model. Am Min 101:627–643. https://doi.org/10.2138/am-2016-5305

45. Stern R, Johnson PR (2010) Continental lithosphere of the Arabian Plate: a geologic, petrologic, and geophysical synthesis. Earth-Sci Rev. https://doi.org/10.1016/j.earscirev.2010.01.002

46. Streck MJ (2008) Mineral textures and zoning as evidence for open system processes. Rev Mineral Geochem 69:595–622. https://doi.org/10.2138/rmg.2008.69.15

47. Takach MK (2018) Quantifying crustal assimilation in historical to recent (1329–2005) Lavas at Mt. Etna, Italy: Insights from Thermodynamic Modeling. Thesis, Central Washington University. https://digitalcommons.cwu.edu/etd/1006

48. Taylor HP Jr (1980) The effects of assimilation of country rocks by magmas of $^{18}O/^{16}O$ and $^{87}Sr/^{86}Sr$ in igneous rocks. Earth Planet Sci Lett. https://doi.org/10.1016/0012-821X(80)90040-0

49. Tepley FJ III, Davidson JP, Tilling RI, Arth JG (2000) Magma mixing, recharge and eruption histories recorded in plagioclase phenocrysts from El Chichón Volcano, Mexico. J Petrol 41:1397–1411. https://doi.org/10.1093/petrology/41.9.1397

50. Tepley FJ III, de Silva S, Salas G (2013) Magma Dynamics and Petrological Evolution Leading to the VEI 5 2000 BP Eruption of El Misti Volcano Southern Peru. J Petrol 54(10):2033–2065. https://doi.org/10.1093/petrology/egt040

51. Tikoff B, Teyssier C (1992) Crustal-scale, en echelon "P-shear" tensional bridges: a possible solution to the batholithic room problem. Geology 20:927–930. https://doi.org/10.1130/0091-7613(1992)020<0927:CSEEPS>2.3.CO;2

52. Ubide T, Kamber BS (2018) Volcanic crystals as time capsules of eruption history. Nat Commun 9:326. https://doi.org/10.1038/s41467-017-02274-w

53. Ubide T, Mollo S, Zhao J, Nazzari M, Scarlato P (2019) Sector-zoned clinopyroxene as a recorder of magma history, eruption triggers, and ascent rates. Geochim Cosmochim Acta 251:265–283. https://doi.org/10.1016/j.gca.2019.02.021

54. Villiger S, Müntener O, Ulmer P (2007) Crystallization pressures of mid-ocean ridge basalts derived from major element variations of glasses from equilibrium and fractional crystallization experiments. J Geophys Res. https://doi.org/10.1029/2006JB004342

55. Wade JA, Plank T, Hauri EH, Kelley KA, Roggensack K, Zimmer M (2008) Prediction of magmatic water contents via measurement of H_2O in clinopyroxene phenocrysts. Geology 36:799–802. https://doi.org/10.1130/G24964A.1

56. Walker JA, Williams SN, Kalamarides RI, Feigenson MD (1993) Shallow open-system evolution of basaltic magma beneath a subduction zone volcano: the Masaya Caldera Complex, Nicaragua. J Volcanol Geotherm Res 56:379–400. https://doi.org/10.1016/0377-0273(93)90004-B

57. Wark DA, Hildreth W, Spear FS, Cherniak DJ, Watson EB (2007) Pre-eruption recharge of the Bishop magma system. Geology 35:235–238. https://doi.org/10.1130/G23316A.1

58. Weber G, Castro JM (2017) Phase petrology reveals shallow magma storage prior to large explosive silicic eruptions at Hekla volcano, Iceland. Earth Planet Sci Lett 466:168–180. https://doi.org/10.1016/j.epsl.2017.03.015

59. Wiebe RA (1968) Plagioclase stratigraphy; a record of magmatic conditions and events in a granite stock. Am J Sci 266:690–703. https://doi.org/10.2475/ajs.266.8.690

60. Wooden JL, Czamanske GK, Fedorenko VA, Arndt NT, Chauvel C, Bouse RM, King BW, Knight RJ, Siems DF (1993) Isotopic and trace-element constraints on mantle and crustal contributions to Siberian continental flood basalts, Noril'sk area, Siberia. Geochim Cosmochim Acta 57:3677–3704. https://doi.org/10.1016/0016-7037(93)90149-q

61. Yoder HS, Tilley CE (1962) Origin of basalt magmas: an experimental study of natural and synthetic rock systems. J Petrol 3:342–532. https://doi.org/10.1093/petrology/3.3.342